Beaufort Gyre freshwater reservoir:
State and variability from observations

Andrey Proshutinsky,[1] Richard Krishfield,[1] Mary-Louise Timmermans,[1] John Toole,[1]
Eddy Carmack,[2] Fiona McLaughlin,[2] William J. Williams,[2] Sarah Zimmermann,[2]
Motoyo Itoh,[3] and Koji Shimada[3]

[1] We investigate basin-scale mechanisms regulating anomalies in freshwater content (FWC) in the Beaufort Gyre (BG) of the Arctic Ocean using historical observations and data collected in 2003–2007. Specifically, the mean annual cycle and interannual and decadal FWC variability are explored. The major cause of the large FWC in the BG is the process of Ekman pumping (EP) due to the Arctic High anticyclonic circulation centered in the BG. The mean seasonal cycle of liquid FWC is a result of interplay between the mechanical (EP) and thermal (ice transformations) factors and has two peaks. One peak occurs around June–July when the sea ice thickness reaches its minimum (maximum ice melt). The second maximum is observed in November–January when wind curl is strongest (maximum EP) and the salt input from the growing ice has not yet reached its maximum. Interannual changes in FWC during 2003–2007 are characterized by a strong positive trend in the region varying by location with a maximum of approximately 170 cm a^{-1} in the center of EP influenced region. Decadal FWC variability in the period 1950–2000 is dominated by a significant change in the 1990s forced by an atmospheric circulation regime change. The center of maximum FWC shifted to the southeast and appeared to contract in area relative to the pre-1990s climatology. In spite of the areal reduction, the spatially integrated FWC increased by over 1000 km^3 relative to climatology.

1. Introduction

[2] The state of the Arctic Ocean and its influence on the global climate system strongly depend on the freshwater budget. Changes in the freshwater balance influence the extent of the sea ice cover, the surface albedo, the energy balance, the temperature and salinity structure of the water masses, and biological processes. The first reasonably comprehensive estimates of the Arctic Ocean salt and heat balances were published by *Timofeev* [1960] and later by *Mosby* [1962]. Both authors considered all possible sources and sinks of freshwater and attempted to balance them using the relatively sparse observational information available at that time. Unfortunately, there remains substantial uncertainty in current estimates of Arctic Ocean freshwater content (FWC) and its seasonal and interannual variability.

The significance of this statement, which has repeatedly concluded all earlier [*Timofeev*, 1960; *Mosby*, 1962; *Coachman and Aagaard*, 1974; *Aagaard and Greisman*, 1975; *Aagaard and Carmack*, 1989] and recent [*Carmack*, 2000; *Serreze et al.*, 2006; *White et al.*, 2007; *Carmack et al.*, 2008] studies of the Arctic Ocean freshwater balance, is increasing with societal demand to explain the rapidly changing Arctic climate.

[3] Investigations of the freshwater balance are closely related to the "Toward an ice-free Arctic Ocean" theme that has been considered and discussed by generations of Arctic scientists [e.g., *Zubov*, 1943; *Budyko*, 1969; *Aagaard and Coachman*, 1975; *Stroeve et al.*, 2007]. Such studies have pointed out that the volume of freshwater stored in the Arctic Ocean and its vertical distribution (ice thickness and concentration, cold oceanic halocline thickness and strength) are regulated by atmospheric dynamics and thermodynamics, freshwater sources and sinks, and ocean circulation and mixing processes (the key processes influencing Arctic climate).

[4] Substantial international interest in Arctic Ocean FWC developed in the 1970s, driven by the Former Soviet Union plans to divert Siberian Rivers for additional irrigation of Kazakhstan and Central Asia. A series of publica-

[1]Woods Hole Oceanographic Institution, Woods Hole, Massachusetts, USA.
[2]Institute of Ocean Sciences, Fisheries and Oceans Canada, Sidney, British Columbia, Canada.
[3]Japan Agency for Marine-Earth Science and Technology, Yokosuka, Japan.

tions [e.g., *Aagaard and Coachman*, 1975; *Semtner*, 1987] discussed potential changes in Arctic conditions that might arise as a result of the expected reductions in river runoff, and the consequential reduction in the strength of the oceanic cold halocline and vertical stability of the upper ocean. Further studies highlighted the impact that freshwater exported from the Arctic Ocean has on deepwater formation at subpolar latitude and in turn, the intensity of the Atlantic Ocean Meridional Overturning Circulation (MOC) [*Aagaard et al.*, 1985; *Lazier*, 1980; *Clarke and Gascard*, 1983; *Talley and McCartney*, 1982; *Dickson et al.*, 1988; *Hakkinen*, 1993, 1999; *Curry and Mauritzen*, 2005; *Rennermalm et al.*, 2006].

[5] Significant changes in the freshwater flux from the Arctic Ocean were documented by *Dickson et al.* [1988]; most notable was the "Great Salinity Anomaly" (GSA). The GSA appeared in the Greenland Sea in 1968 and circulated around the subpolar ocean for at least 15 years. Various explanations for the GSA have been offered [*Dickson et al.*, 1988; *Walsh and Chapman*, 1990; *Mysak et al.*, 1990; *Hakkinen*, 1993, 1999]. *Proshutinsky and Johnson* [1997] gave evidence that such salinity anomalies may originate inside the Arctic Ocean because of a redistribution of freshwater. *Belkin et al.* [1998] revisited the GSA of the 1970s and documented the existence of two additional subpolar salinity anomalies in the 1980s and 1990s.

[6] Other interesting results were obtained from modeling studies by *Delworth et al.* [1993, 1997] who pointed out that salinity anomalies in the Arctic Ocean surface layer precede anomalies of the MOC intensity by 10–15 years. *Hakkinen* [1993] examined the cause of salinity anomalies using a 3-D coupled ice-ocean model and concluded that strong northerly winds over the Greenland Sea and Fram Strait area lead to an increase in the thick ice transport from the Arctic Ocean and to increased freshwater discharge. While analyses of observational data by *Wohlleben and Weaver* [1995], *Walsh and Chapman* [1990], and *Mysak and Venegas* [1998] supported *Hakkinen*'s [1993] model results, the possible contribution of liquid freshwater to the flux increase was not considered.

[7] Another development in the investigation of the Arctic Ocean freshwater budget and its variability began in the 1990s following a decision by the Arctic Ocean Sciences Board (AOSB) in July 1996 to organize a "Symposium on the Freshwater Balance of the Arctic." These activities resulted in the NATO advanced research workshop "The Freshwater Budget of the Arctic Ocean," Tallinn, Estonia, 27 April to 1 May 1998. The workshop proceedings [*Lewis*, 2000] outlined the state and variability of the Arctic Ocean freshwater budget including a traditional investigation of the freshwater budget of the Arctic Ocean (i.e., detailed analysis of its major components including river runoff, inflow from the Atlantic and Pacific oceans, outflows through Fram Strait and the Canadian Archipelago, the atmospheric moisture flux, and the annual cycle of ice formation and melt). A comprehensive inventory of the freshwater budget of the Arctic Ocean was also presented by *Carmack* [2000]. The report from a later meeting of the AOSB (http://www.aosb.org/mtgs/ XVII.html) included recommendations to (1) study shelf processes contributing to the formation of sea ice and of

dense bottom water; (2) study the outflow of freshwater and ice through the Canadian Archipelago; (3) study the impact of a reduction or cutoff of Pacific inflow; and (4) continue to monitor the total FW exchange with the North Atlantic (NA), including the export of ice. Most of these recommendations have been implemented by the international ASOF program (Arctic-Subarctic Ocean Fluxes [*Dickson et al.*, 2008]) that has as its major objectives to measure and model variability of fluxes between the Arctic Ocean and the Atlantic Ocean and to understand the role of these fluxes in decadal climate variability. The recent results of *Serreze et al.* [2006] and *White et al.* [2007] refine some of the numbers in the accepted mean Arctic Ocean freshwater budget, but they did not fully resolve its seasonal, interannual and decadal variability, nor identify mechanisms responsible for changes.

[8] The general approach to freshwater studies by the AOSB, ASOF and other investigators assumes a priori that the inflow and outflow of freshwater are balanced at any given time. Little attention has been given to the mechanisms of freshwater storage in the Arctic Ocean and its variability. Our approach to the FWC problem, formulated by *Proshutinsky et al.* [2002] (hereinafter referred to as *P*2002), allows for imbalance between the numerous sources and sinks of freshwater in the Arctic Ocean. That is, we allow that the Arctic Ocean can accumulate a significant volume of freshwater during one climate regime and later release it to the Greenland, Iceland, and Norwegian Seas and NA during another climate state or circulation regime. This tenet has allowed us to formulate several hypotheses to explain salinity anomalies in the NA and decadal variability of the Arctic climate [*P*2002; *Dukhovskoy et al.*, 2004, 2006].

[9] The largest freshwater storage area of the Arctic Ocean is located in the Beaufort Gyre: identified by a regional salinity minimum at depths of 5–400 m (Figure 1) [see also *P*2002; *Proshutinsky et al.*, 2009]. Existence of the Beaufort Gyre (BG) freshwater reservoir was inferred by *P*2002 via an analysis of salinity fields, wind, and ice drift patterns. *P*2002 hypothesized that in winter, the wind (a dynamic factor) drives the ice and ocean in a clockwise sense and the BG accumulates freshwater mechanically through a deformation of the salinity field (Ekman convergence and associated downwelling). In summer, winds are weaker (and may even reverse to be counterclockwise). The resultant anomaly in Ekman convergence releases freshwater, relaxes salinity gradients and reduces the BG FWC. *P*2002 tested this mechanical hypothesis for freshwater accumulation and release by employing a relatively simple model where wind was the major driving force (the influences of sea ice and ocean thermodynamics were neglected). They further pointed out that thermodynamical processes may also be important: in winter, ice growth and subsequent salt release reduce the (liquid) FWC of the BG, and in summer, ice melt increases the FWC. The interplay between dynamic and thermodynamic forcing is clearly complicated. Another factor likely to be important and not considered by *P*2002 is the change in FWC associated with the advection of surface, Pacific, and Atlantic waters into the BG.

[10] In this paper, we attempt to address questions and test hypotheses formulated by *P*2002 associated with BG
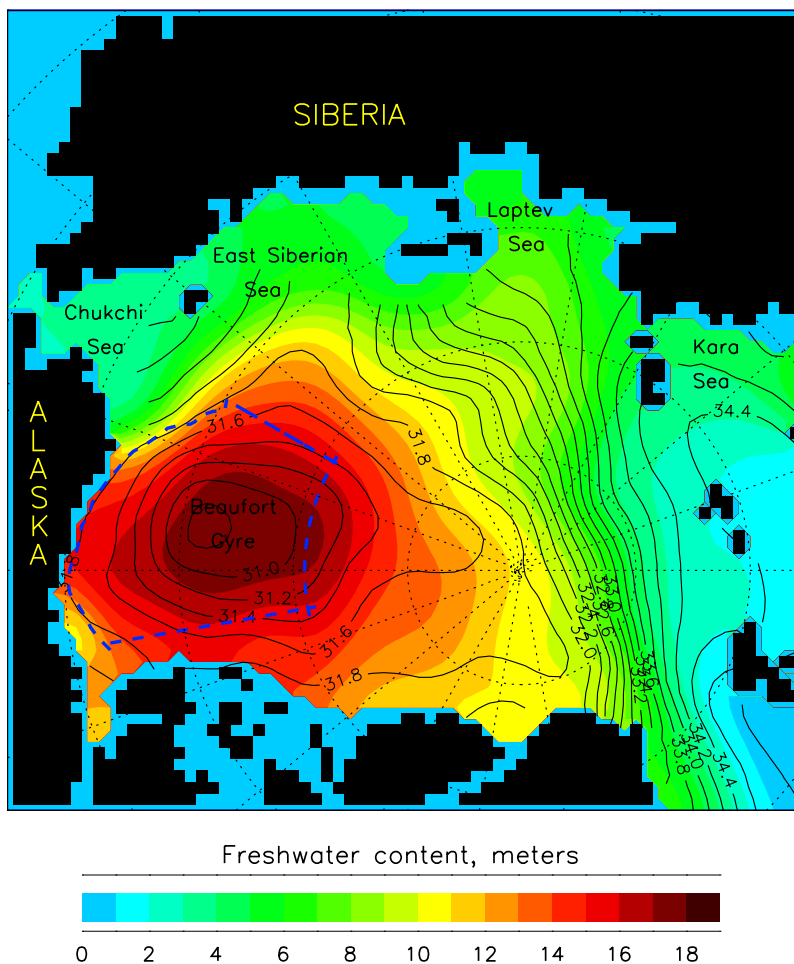
Figure 1. Climatology of freshwater content in the Arctic Basin (shown in colors). Solid lines depict mean 1950–1980 salinity at 50 m. Freshwater content is calculated relative to salinity 34.8 on the basis of 1950–1980 data from *Timokhov and Tanis* [1998] averaged for all decades. The Beaufort Gyre Region (BGR) is bounded by thick dashed blue lines.

FWC variability at seasonal to decadal timescales. We investigate basin-scale mechanisms regulating FWC in the BG area using measurements from the 2000s obtained by the BG Exploration Project and by drifting Ice-Tethered Profilers (ITPs), historical observations from the 1950s to the 1980s from *Timokhov and Tanis* [1997, 1998], and data collected in the 1990s by different national and international expeditions. Section 2 describes the data sources and our methodology of FWC estimation from the historical gridded and bottle data, and from conductivity-temperature-depth (CTD) profiles (shipboard, moored profilers and profiles from drifting buoys). FWC variability on seasonal, interannual and decadal timescales is analyzed in sections 3 and 4. Major findings are summarized in section 5.

2. Study Area, Methods, and Data Sources

[11] To facilitate temporal comparisons of BG integral parameters, we define the Beaufort Gyre Region (BGR) in terms of the climatologic location of the gyre as bounded by 70.5°N to 80.5°N and 130°W to 170°W (Figure 1). FWC calculations were carried out for this region at grid points having total depths greater than 300 m.

2.1. Freshwater Content Calculations

[12] Freshwater content (liquid) (FWCL) (m) in the ocean is calculated as

$$\mathrm{FWCL} = \int_{z2}^{z1} \frac{[Sref - S(z)]}{Sref} dz, \tag{1}$$

where the z axis is defined as positive up with the surface $z = 0$. The reference salinity, $Sref$ is taken as 34.8; $S(z)$ is the salinity of the water at depth z. We take $z2$ as the depth level where $S(z) = Sref$ while $z1$ defines the upper level of the FWCL integrations. For total water column FWCL, $z1 = 0$. Change in FWCL is thus a measure of how much liquid freshwater has accumulated or been lost from the ocean column bounded by the 34.8 isohaline and $z = z1$. (See *Aagaard and Carmack* [1989], *Carmack* [2000], and *Carmack et al.* [2008] for details on the significance of the reference salinity in the analysis of FWCL.)

[13] The FWC in sea ice (FWCI or solid) is formally given by equation (2)

$$FWCI = \int_{zice}^{0} \frac{[Sref - Sice]}{Sref} dz + \int_{0}^{fb} \frac{[Sref - Sice]}{Sref} dz. \quad (2)$$

Here, $zice$ is the draft of the sea ice that we measured using Upward Looking Sonars (ULSs); fb is the freeboard of the sea ice. The freeboard can be measured by satellites but in this paper we calculate sea ice thickness (Hi, which is $zice$ + fb) from the sea ice draft as $Hi = zice(\rho w/\rho i)$, where ρi and ρw are ice and water densities, respectively. Assuming vertically uniform sea ice salinity ($Sice$) of 1.8 according to *Perovich et al.* [2009], the FWCI is calculated as

$$FWCI = 0.948 Hi. \quad (3)$$

For snow FWC calculations we follow the recommendations of *Sturm et al.* [2002] who analyzed the evolution and spatial distribution of the snow cover on the Arctic sea ice during the Surface Heat Budget of the Arctic Ocean (SHEBA) project. Specifically we assume that the snow has no salt and that the snow water equivalent, $SWE = 0.343 Hsn$ where Hsn is snow thickness.

2.2. Interpolation Technique

[14] Optimal interpolation (OI) was used to construct spatial maps (on a 50-km square grid) of the freshwater distribution in summer for the decades of the 1990s and 2000s and each year from 2003 through 2007 using all available CTD stations and ITP profiles, between the last week of June and first week of October (inclusive). The decadal interpolations ignore interannual variability and combine all available data for the whole decade from the summer months. Sufficient spatial coverage of observations since 2003 allowed optimal interpolations to be constructed for each year up through 2007. The optimal interpolation method improves on earlier methods used to calculate the same quantities [e.g., *Carmack et al.*, 2008], because it uses statistics from the data to minimize the mean square error of the interpolated estimates, and produces an objective estimate of the expected error. The OI method [e.g., *Gandin*, 1965; *Bretherton et al.*, 1976; *Reynolds and Smith*, 1994; *Emery and Thomson*, 1997] is based on the assumptions that the statistics of the data being mapped are stationary, homogeneous, and isotropic. Values are calculated at grid points from the averages weighted by the distance from each observation. The weights are proportional to the covariability of the data which in our application was calculated from the observations and could be approximately represented by a Gaussian function with length scale of 300 km.

[15] In addition to the raw data locations, desired grid locations, and covariance length scale, the method requires a starting reference background field and estimates of the error in the raw measurements (0.2 m is allowed in our OI generated maps) and variance of the observations for determining expected error estimates. The OI mapping procedure is applied to anomalies from the reference field and the result is added back to the reference to produce the final map. Specifying a realistic reference field is particularly important to the results away from the raw data locations, because at such sites, the OI technique returns estimates that approach the reference field values. Climatological estimates are often used as the reference field in geophysical applications, but could not be used here since preliminary analysis indicated that there was significant change in the freshwater distribution in the BGR in the 1900s from the best available climatology [*Timokhov and Tanis*, 1997, 1998]. Furthermore, our region was only sparsely sampled in the decade preceding the first year of the BG program. Consequently, in this application it was necessary to construct a best guess reference field estimate for the 1990s and for the first year of the BG program (2003) from the data themselves (supplemented with observations from 2002 to enhance spatial coverage). A polynomial surface fitting algorithm (as in the paper by *Carmack et al.* [2008]) was used to construct the base map for 2003 using raw data from 2002 to 2003. In subsequent years, the calculated OI map of FWC from the previous year was used as the base map.

[16] A map of the multiyear mean FWC distribution during the Beaufort Gyre Observational System (BGOS) (http://www.whoi.edu/beaufortgyre) time period was obtained as the average of the annual maps from 2003 to 2007; error for the 5-year time period was computed from the OI determined mean error for all years. Estimates of the interannual trend in FWC were derived from linear regressions at each grid cell of the same annual maps.

2.3. Data Sources
2.3.1. Ocean and Sea Ice Data From the Beaufort Gyre Observing System (2003–2007)

[17] Beginning in August 2003, time series measurements of temperature, salinity, currents, geochemical tracers, sea ice draft, and sea level have been acquired in the BGR by a team of Woods Hole Oceanographic Institution investigators in collaboration with scientists from Fisheries and Oceans Canada, Institute of Ocean Sciences and the Japan Agency for Marine-Earth Science and Technology under the JWACS (Joint Western Arctic Climate Studies) and BGEP (Beaufort Gyre Exploration Project supported by the U.S. National Science Foundation) activities consisting of a series of BGOS expeditions (Figure 2). Observations of ocean temperature and salinity (T&S) were obtained from moorings, drifting buoys, and shipboard instruments. Standard hydrographic sections consisting of fixed sites revisited annually (August–September) have allowed investigation of interannual variability of measured parameters in the BGR during summer. The mooring data allow estimation of sea level variability, sea ice draft and variations in the

Figure 2. The composition of the Beaufort Gyre Observing System (BGOS) by year. Large yellow circles show mooring locations (A, B, C, and D indicated), small white circles show locations of CTD stations, white crosses depict locations of XCTD castings, and colored lines depict ITP trajectories. Background colors show bathymetry from *Jakobsson et al.* [2000]. Vectors show mean 1979–2000 ice drift pattern.
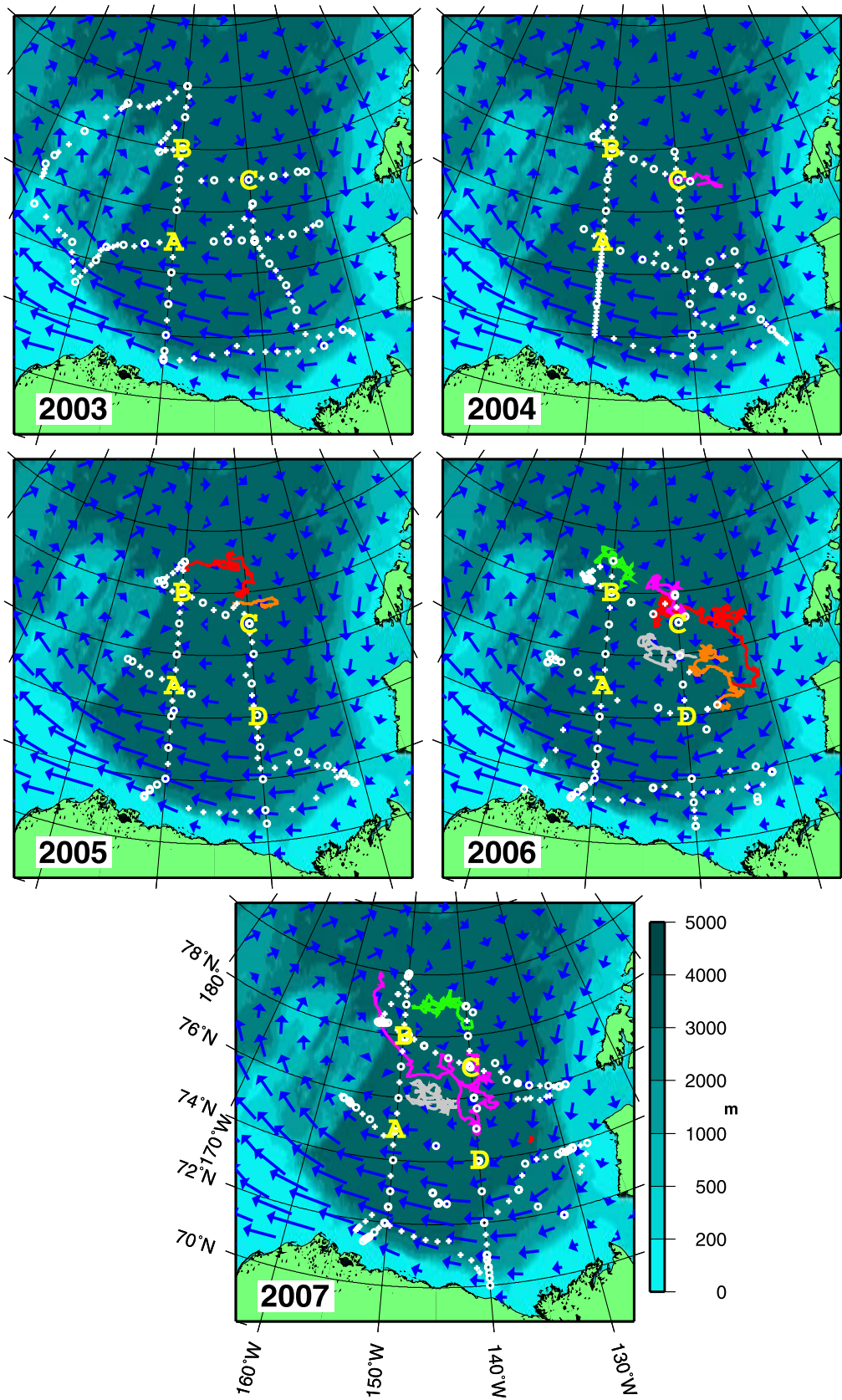
Beaufort Gyre Observing System

Figure 2

vertical distribution of FWC at three (and later four) locations throughout the year (Figure 2). In addition, eight Ice-Tethered Profilers (ITPs) (Figure 2) measuring T&S daily at depths ranging between ~7 and 760 m have returned year-round information from the BGR in real time via satellite (see *Krishfield et al.* [2008] and ITP project web site (http://www.whoi.edu/itp) for more details).

[18] Time series of freshwater content at fixed location spanning the entire annual cycle are derived from salinity profiles acquired by BGOS bottom-anchored moored profiler instrumentation (McLane Moored Profiler (MMP)). MMP data acquisition followed a burst sampling scheme consisting of two one-way profiles separated in time by 6 h initiated every 48 h. To avoid collision with ice keels, the tops of the moorings were positioned at or deeper than 45 m below the surface. On moorings A and C in 2003, the MMPs profiled between 95 m and 2000 m, while for all other moorings and years the MMPs profiled between 65 m and 2000 m. Three of the BGOS moorings (A, B, and C) have been continuously maintained since 2003; mooring D was first installed in 2005. As documented by *Ostrom et al.* [2004], MMP salinity data are believed to have an uncertainty of less than 0.005; resultant errors in FWCL estimates (for depth intervals sampled by the MMPs) are less than 0.1 m.

[19] As above, the high-accuracy shipboard salinity measurements result in FWCL uncertainties for individual profiles of less than 0.1 m. Our calculations of interpolation errors for the 2003–2007 hydrographic surveys estimate that the expected error varies from 0.1 m to 1.5 m depending on the distance a given grid point is from that year's observations.

[20] Eight ITP instruments returned approximately 7200 T&S profiles from the BGR in the 2004–2007 time period (Figure 2). Typically, each system occupied two vertical profiles per day between 7 m and 760 m depth. After calibration, the accuracies of the ITP salinity data are believed to be comparable to those from the ship-based and bottom-moored instruments [*Krishfield et al.*, 2008]. In order to construct FWCL estimates integrated to $z1 = 0$, a method was needed to extrapolate upward the MMP and ITP profiles. A scaling procedure was developed, described in Appendix A, to reconstruct FWC in the upper ocean. Because the ITPs typically sampled from 760 m and up to 7 m depth, uncertainty in the ITP-full water column FWC estimates from vertical extrapolation is relatively small (no worse than 0.50 m in summer, decreasing to zero in winter when the ITPs sampled up into the surface mixed layer). In turn, uncertainty in the reconstructed mooring FWC estimates (0.50 m) was quantified by referencing the CTD and ITP data collected near the moorings (see Appendix A for details). Last, in order to differentiate temporal and spatial variability in the drifting ITP observations, we developed an FWC anomaly estimation procedure relative to a reference spatial map. The technical issues are discussed in Appendix A.

[21] The expected error of our sea ice FWC calculations derives from errors in the sea ice draft measurements (~0.10 m), errors associated with sea ice salinity (±1) and errors related to sea ice density ±20 kg m^{-3} [*Perovich et al.*, 2009]. Fortuitously, the errors in sea ice density and salinity

compensate each other in the sea ice FWC calculations; we assume that the total error in FWCI is ±0.10 m.

[22] The expected FWC errors due to snow water equivalent calculations are comparable with errors in sea ice FWC computations. For the entire winter, the mean snow depth at the SHEBA site was 0.337 m, giving a mean snow water equivalent of 0.116 m [*Sturm et al.*, 2002]. This snow was accumulated until end of May and then started melting. Observations of snow depth in the BGR by the Ice Mass Balance Buoys [*Richter-Menge et al.*, 2006] show that the mean snow depth in 2003–2004 was 0.26 m with snow water equivalent of 0.089 m and the snow typically started melting in early June. Taking into account that sea ice draft changes recorded by ULSs include changes due to snow on the sea ice surface (~0.10 m in water equivalent during seasonal cycle) we assume that the snow contribution to uncertainty in our FWC estimates is encompassed by the estimated error in sea ice thickness.

2.3.2. Ocean Data From 1990s

[23] Hydrographic T&S surveys from the 1990s and early 2000s used in this study were obtained from Fisheries and Oceans Canada, Institute of Ocean Sciences, the Japan Agency for Marine-Earth Science and Technology, and the National Snow and Ice Data Center and National Oceanographic Data Center, including data from the SCICEX (Scientific Ice Expeditions, 1993–1998 that occupied repeat expendable CTD (XCTD) transects) and SHEBA (1997–1998) expeditions.

[24] In calculations of decadal-averaged FWC for the 1990s when CTD and XCTD data were used, there are instances where the available T&S profiles do not extend fully to the ocean surface. For example, the SCICEX XCTDs typically only sampled below 25 m depth. In these cases, the shallowest salinity value in a profile was extended uniformly to the surface. Given that the typical wintertime mixed layer depth in the BG is at least 25 m deep, this extrapolation results in a very small error in FWC (<0.20 m). However, in summer when mixed layers are thinner, this extrapolation may result in an underestimation of FWC by as much as 1.0 m (quantified using 1-m resolution shipboard CTD data). The accuracy of calibrated CTD salinity data from this decade is estimated to be better than 0.01, which translates to a total FWC anomaly uncertainty of less than 0.10 m. However, transient surface variations and other uncertainties inherent in the data from the shallowest sampled layer more likely limit the overall accuracy of an FWC estimate from any single profile to 0.50 m. As indicated earlier, we use 0.20 m to quantify the accuracy of the measurements for producing the optimal grids.

2.3.3. Ocean T&S Climatology

[25] Historical summer T&S gridded data for this region are taken from *Timokhov and Tanis* [1998]. *Timokhov and Tanis*'s [1997, 1998] gridded fields are used to calculate liquid FWC distributions for the decades from the 1950s through the 1980s. It should be noted that the historical data are most extensive during the 1970s [*Timokhov and Tanis*, 1997, 1998], reflecting mostly winter conditions when Soviet aircraft could land on the ice. *Timokhov and Tanis*'s [1997, 1998] data are based primarily on bottle data and are provided at standard levels after smoothing and interpolation. The accuracy of the salinity measurements from the
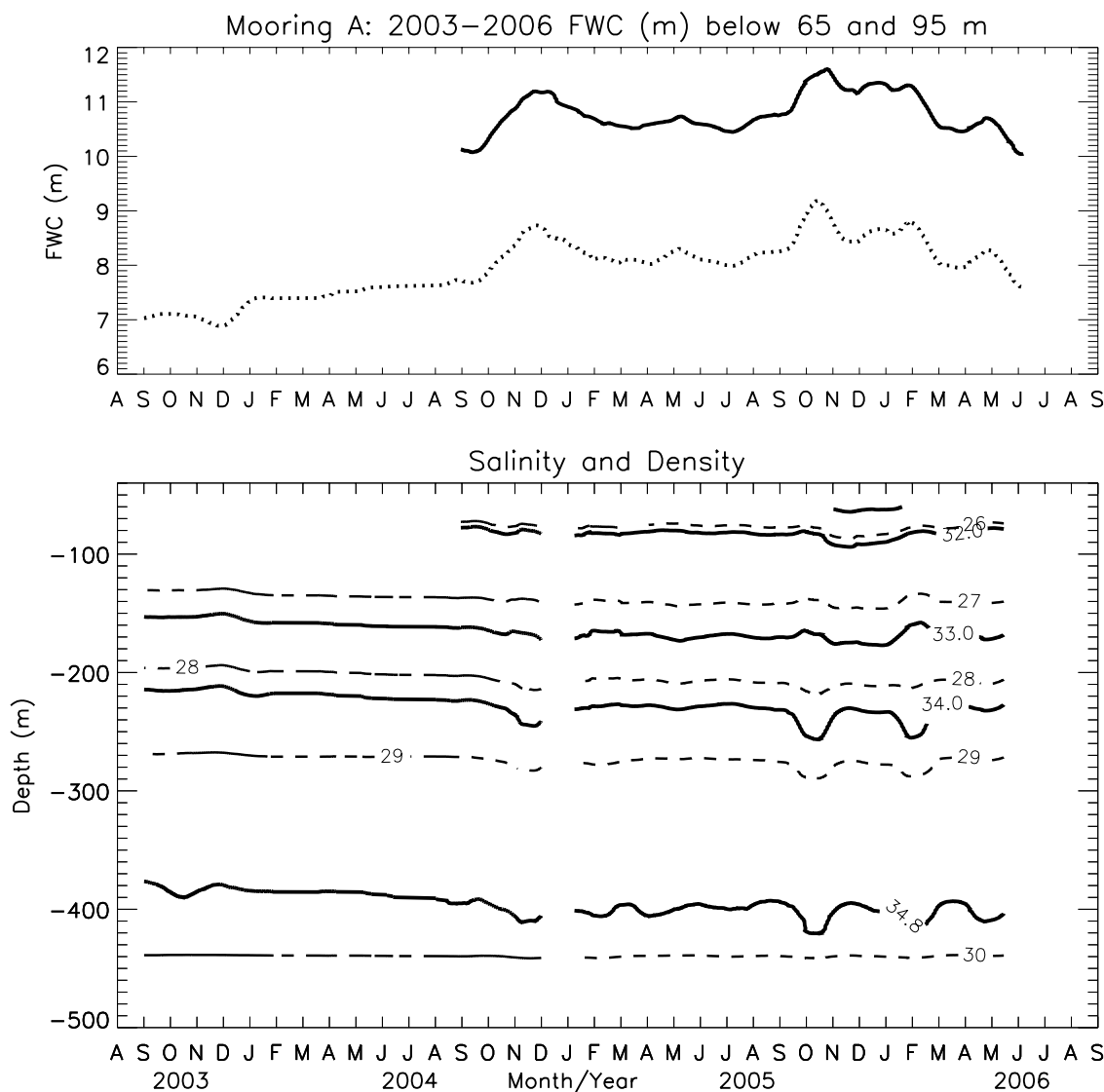
Figure 3a. (top) The 15-day running mean FWC (m) time series below 65 m (solid line) and 95 m (dotted line) from MMP at BGOS mooring A (75°N, 150°W) from summer 2003 to summer 2006. (bottom) The 15-day running mean seawater salinity (solid lines) and density (dashed lines) contours versus depth.

bottle data is estimated as 0.02. The errors in FWC associated with measurement accuracies and use of measurements at standard levels is less than 0.50 m. These errors were estimated by comparing FWC estimates on the basis of CTD data with 1-m vertical resolution to FWCs calculated from standard *Timokhov and Tanis* [1997, 1998] levels. *Timokhov and Tanis*'s [1997, 1998] product contains interpolated fields along with some information about interpolation errors which for salinity are reported to vary between 0.02 to 0.05. Assuming a worst-case scenario that these errors exist in all layers of the ocean, the maximum error in FWC due to interpolation will be between 0.20 to 0.45 m.

2.3.4. Atmosphere and Satellite-Based Sea Ice Data

[26] Complementing the in situ measurement programs, remote sensing projects and atmospheric reanalysis data are also utilized in the present analysis. Sea ice concentration data are taken from *Comiso* [1999] and sea ice drift parameters from *Fowler* [2003], both updated and available

from the National Snow and Ice Data Center (NSIDC). Sea level pressure (SLP) data from the National Center for Atmospheric Research and National Centers for Environmental Predictions (NCAR/NCEP) reanalysis are also used, along with geostrophic winds and surface wind stresses calculated from SLP to characterize the atmospheric forcing.

3. Beaufort Gyre Region Freshwater Content Interannual and Seasonal Variability in 2000s

3.1. Observational Results From Moorings

[27] Investigation of the interannual and seasonal variability in solid (ice) and liquid (ocean) FWC is important to understand the mechanisms responsible for the BG freshwater accumulation and release processes, their timing and scales of changes. Historical observations are limited in the BGR that is covered with sea ice year-round, making it impossible to reconstruct the record of interannual and
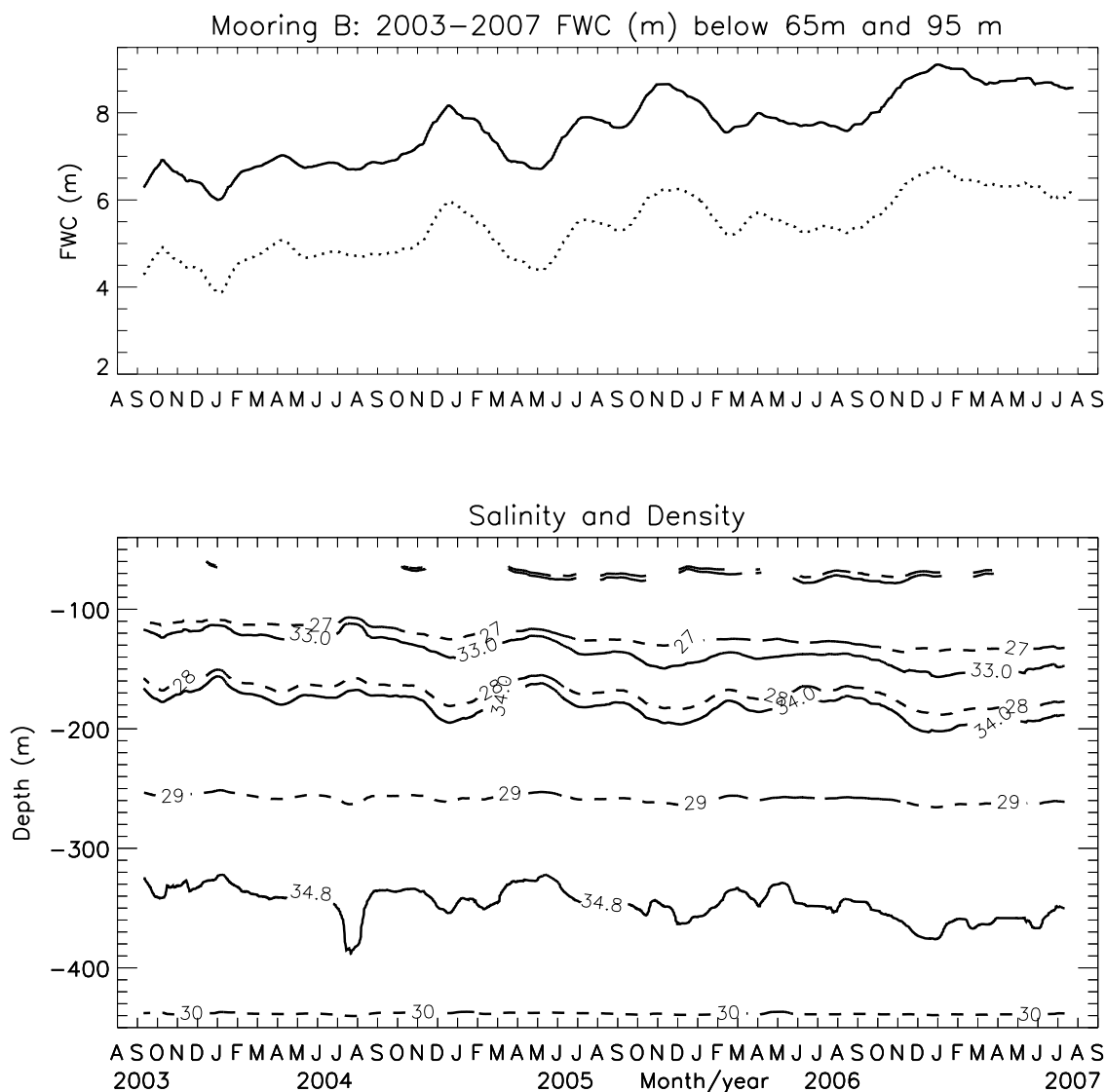
Figure 3b. Same as in Figure 3a but for mooring B (78°N, 150°W).

seasonal variability of FWC there before the 2000s. But recently, high temporal resolution time series are available from the four BG moorings and ITPs.

[28] Using the BGOS mooring data (MMP profiles), time series of liquid FWC, salinity and water density at moorings A, B, C, and D for the period 2003–2007 were constructed (Figure 3). The data were smoothed using a 15-day running mean procedure although there are still instances where eddy structures influence the FWC estimates (e.g., at mooring A in October 2005). At moorings B and C, the FWC exhibits a positive trend from fall 2003 through 2007 superimposed on seasonal and higher-frequency signals. At mooring A, the FWC has a positive trend for the period 2003–2005. Thereafter, FWC remained roughly constant or decreased (no MMP data were collected at this mooring during the 2006–2007 deployment). Mooring D data span only 2 years, limiting the ability to detect interannual trends. They do, however, indicate that for the 2005–2007 period there is an overall decrease in FWC below 65 m at that

location. Mooring D also shows a very well pronounced seasonal cycle with a peak in FWC in November–December and absolute minima in September–October. The other mooring records also document a FWCL seasonal maxima typically occurring sometime between October and January but the interannual variability is significant.

[29] The FWCL variability reconstructed for the entire water column (see Appendix A for details) shows much larger changes (Figure 4) with significant positive trends in FWCL at all moorings ranging from 64 cm a^{-1} at mooring D to 178 cm a^{-1} at mooring B.

[30] The range of sea ice thickness changes (obtained from ULS records) varies among moorings. The seasonal magnitude of sea ice draft (Figure 4) is approximately 150 cm. The maximum ice draft/thickness in the BGR is observed between May and June and the minimum between late August and early November depending on the year and mooring location.
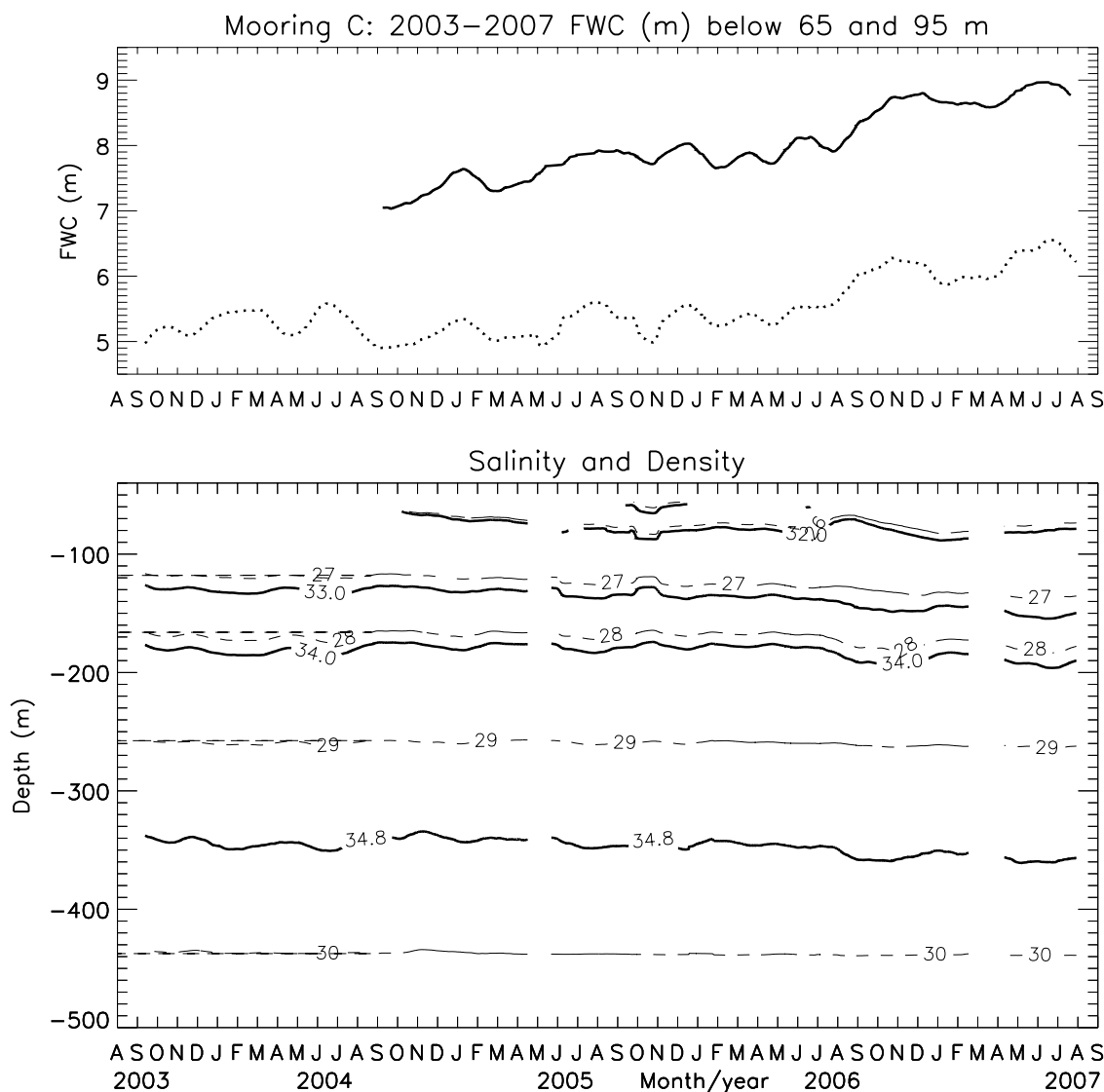
Mooring C: 2003−2007 FWC (m) below 65 and 95 m

Figure 3c. Same as in Figure 3a but for mooring C (77°N, 140°W).

[31] In order to analyze seasonal changes in the FWC we detrended the time series of liquid and solid FWC components and constructed an average seasonal cycle for each mooring location (Figures 5a, 5b, 5c, 5d, 6a, 6b, 6c, and 6d). In general, we observe two peaks in the liquid FWC anomaly during a seasonal cycle, one maximum in December−January and a second, smaller one (less pronounced at mooring A) is typically observed in July−August, depending on mooring location. We can also identify two minima in the liquid FWC anomalies: the first one is typically observed in April−May and the second in September−October. Note however that there is significant interannual variability in the liquid FWC anomalies during the 2000s (Figures 5 and 6).

[32] The sea ice contributions to the liquid FWC variability are well pronounced during a seasonal cycle. Typically, the sea ice starts releasing liquid freshwater into the ocean in the middle of May, and the volume of freshwater from the ice reaches a maximum in the ocean in September−October. Notable however, there is more going on in the BGR FWC seasonal cycle than simple phase change as sizable

anomalies in total FWC (ice plus liquid) are observed (Figures 5e, 5f, 6e, and 6f).

3.2. Causes of Seasonal FWC Changes in 2003−2007

[33] The seasonal cycle of liquid FWC revealed above is not fully consistent with the conventional understanding of the Arctic Ocean hydrological cycle [*Timokhov and Tanis*, 1997, 1998; *Steele et al.*, 2001; *Serreze et al.*, 2006, Figure 11] in which maximum liquid FWC occurs in August and the minimum in April. This understanding was based on an idealized concept of the Arctic without sea ice drift, ocean currents, and mixing. In this simplified case, the seasonal cycle of sea ice growth and melt due to the seasonal changes in solar radiation results in ocean FWC variability influenced only by changes in air temperature [see *Overland*, 2009, Figure 1]. Our results indicate that there are two minima and two maxima in the mean seasonal cycle of BG liquid FWC and only the April minimum coincides with the "climatologic" view point.

[34] Under pure thermodynamic forcing (i.e., without dynamic processes and mixing) the Arctic Ocean would
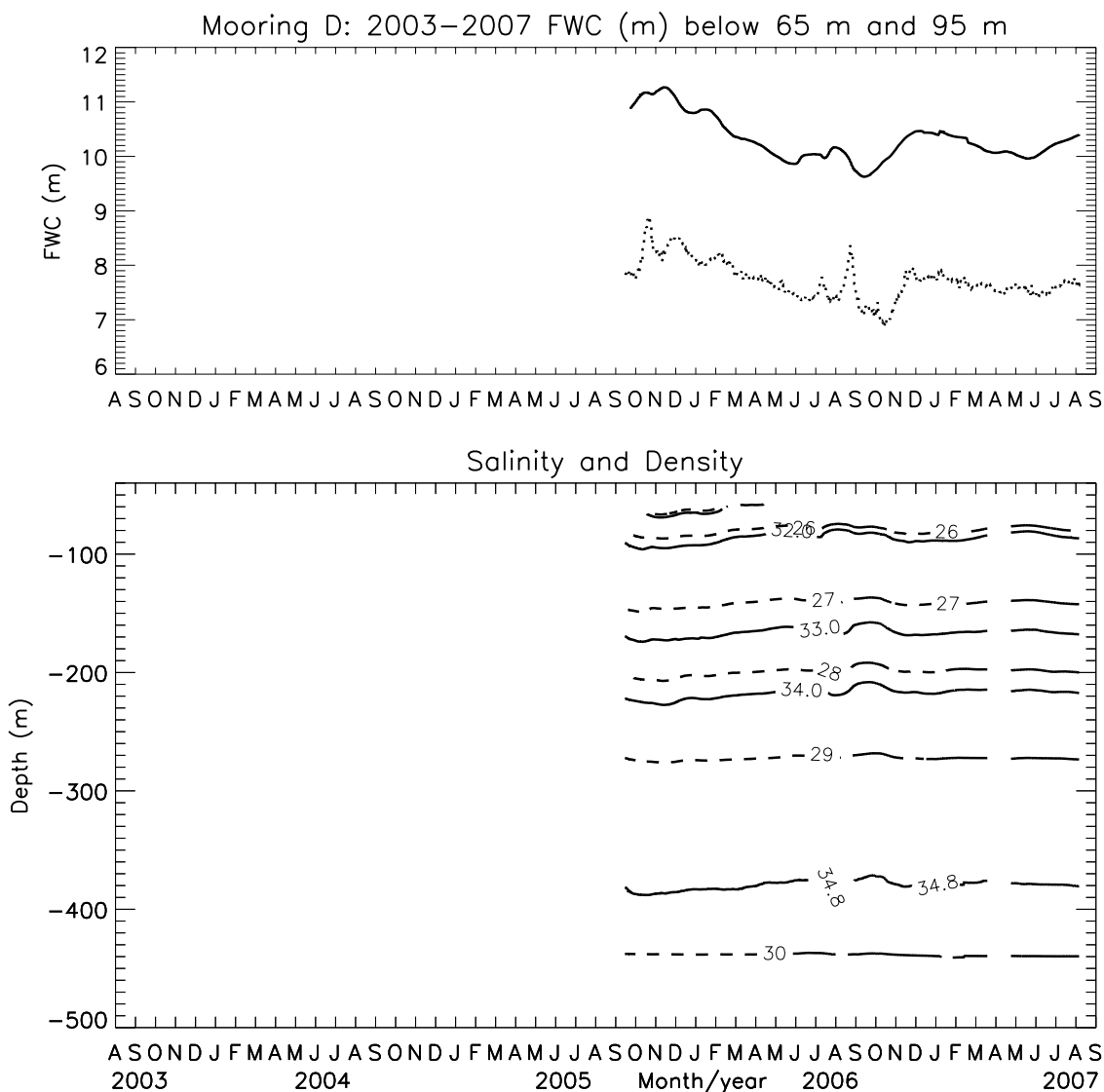
Figure 3d. Same as in Figure 3a but for mooring D (74°N, 140°W).

quickly become a two-layer ocean with a completely fresh upper layer and a salty lower layer (see the description of this distillation process by *Aagaard and Carmack* [1989]). In the real ocean, the seasonal variability in local liquid FWC (*FWCL*) is not only influenced by changes in sea ice seasonal transformations (*FWCI*) under the solar radiation seasonal cycle, but is also forced by changes in Ekman pumping (EP) (*FWCE*), ocean mixing (*FWCM*) and by changes in freshwater sources and sinks (*FWCSS*). The latter includes precipitation, evaporation, river runoff and freshwater fluxes via ocean straits. We may then express *FWCL*(*t*) (where *t* is time) as the sum:

$$FWCL(t) = FWCI(t) + FWCE(t) + FWCM(t) + FWCSS(t). \quad (4)$$

[35] On the basis of (4) we speculate that the Arctic Ocean FWCL seasonal cycle should differ significantly from region to region, complicating assessments and inter-comparisons. For example, in coastal regions influenced most directly by river runoff, the maximum FWCL is observed in the middle of July (following maximum river runoff in June) and the minimum is observed at the end of April (minimum river runoff and maximum landfast ice thickness). Our observations in the BGR indicate that the seasonal freshwater anomalies associated with changes in sea ice thickness (*FWCI*) follow closely the seasonal anomalies of air temperature (Figures 5c, 5d, 6c, and 6d) but do not explain fully the observed seasonal FWCL cycle (Figures 5a, 5b, 6a, and 6b). The influence of freshwater sources and sinks (*FWCSS*) in the formation of summer positive FWCL anomalies in the BGR is questionable because the maximum river runoff and the maximum inflow of the freshwater from the Bering Sea are observed in June– July [*Woodgate et al.*, 2005] and these signals cannot reach the central part of the Beaufort Gyre by August. The seasonal FWC anomalies in precipitation are mostly asso-ciated with snow (rain is very rare in the BGR). The
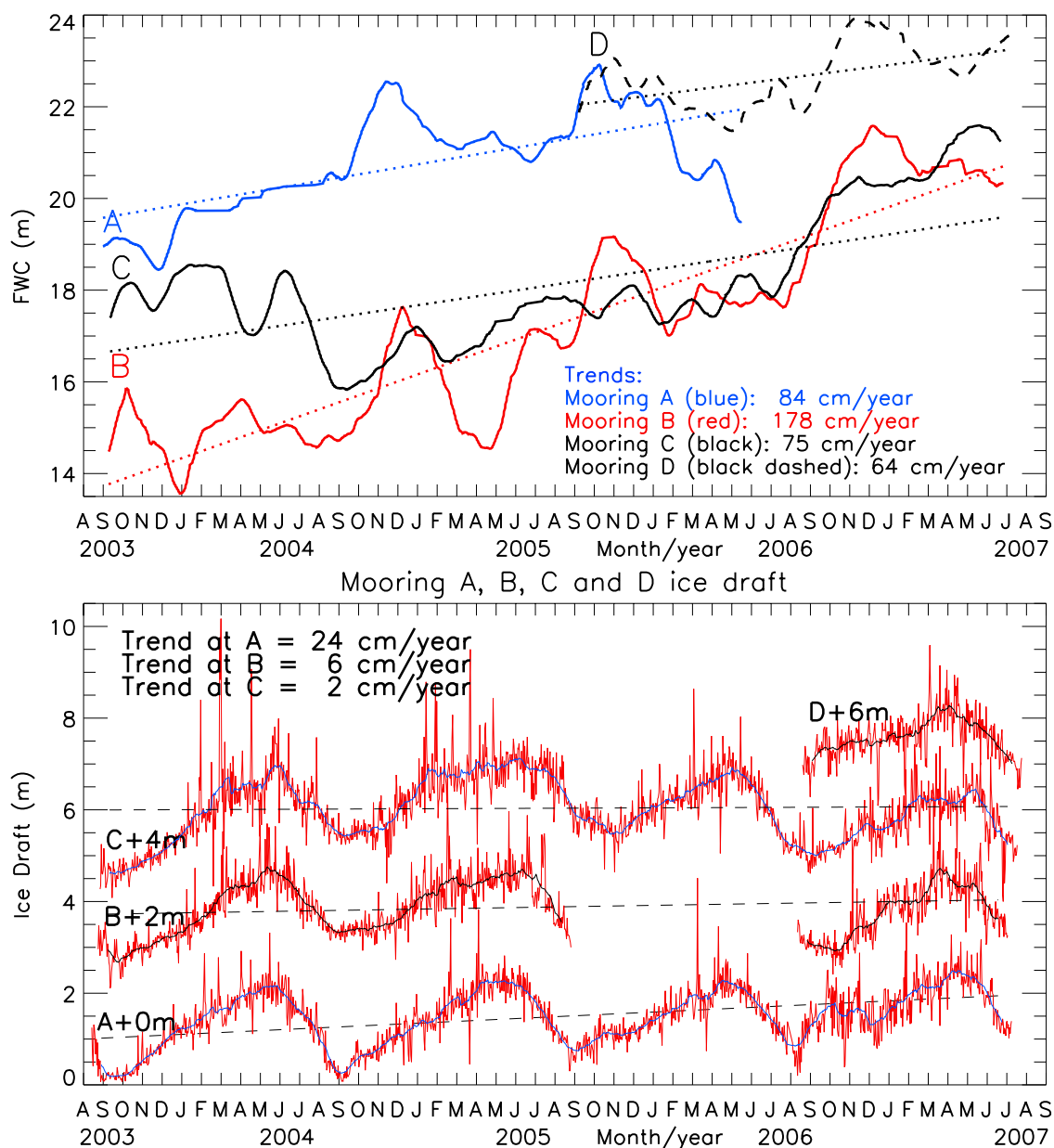
Figure 4. FWCL time series (m) from MMPs using (top) derived FWCL coefficients and (bottom) time series of sea ice draft (m) from Upward Looking Sonars from BGOS moorings for 2003–2007. FWCL trend lines in Figure 4 (top) (dotted) are calculated from the corrected FWC MMP data. Ice draft trends are also shown in Figure 4 (bottom) as dashed black lines. Note that the ice draft data are offset from one another by 2 m.

information about changes in snow depth and snow water equivalent is already taken into account by our sea ice draft measurements as discussed above. Ocean mixing (*FWCM*) is an important factor which is able to preserve freshwater anomalies in the region. It depends on many oceanic internal and external parameters. The majority of them are associated with wind forcing (or sea ice stresses at the ocean surface) and the ocean vertical stratification. For this study we assume that *FWCM* can be included in the term of EP which is also a function of wind stress and ocean stratification.

[36] The EP forcing, which influences freshwater accumulation and release [*Hunkins and Whitehead*, 1992;

*P*2002] in the BGR, was evaluated using time series of wind curl averaged over the BGR or in the vicinity of each mooring. The 2003–2007 NCAR/NCEP Reanalysis 1 wind curl estimates were detrended and a mean seasonal cycle was constructed for each mooring location. The climatologic annual mean wind stress curl over the BGR is negative (not shown) [see *P*2002; *Yang and Comiso*, 2007; J. Yang, Seasonal and interannual variability of EP in the Beaufort Sea, submitted to *Journal of Geophysical Research*, 2009] and the EP is positive leading to the accumulation of FWC in the BG. In the typical seasonal cycle (Figures 5e, 5f, 6e, and 6f) the wind stress curl anomaly usually reaches
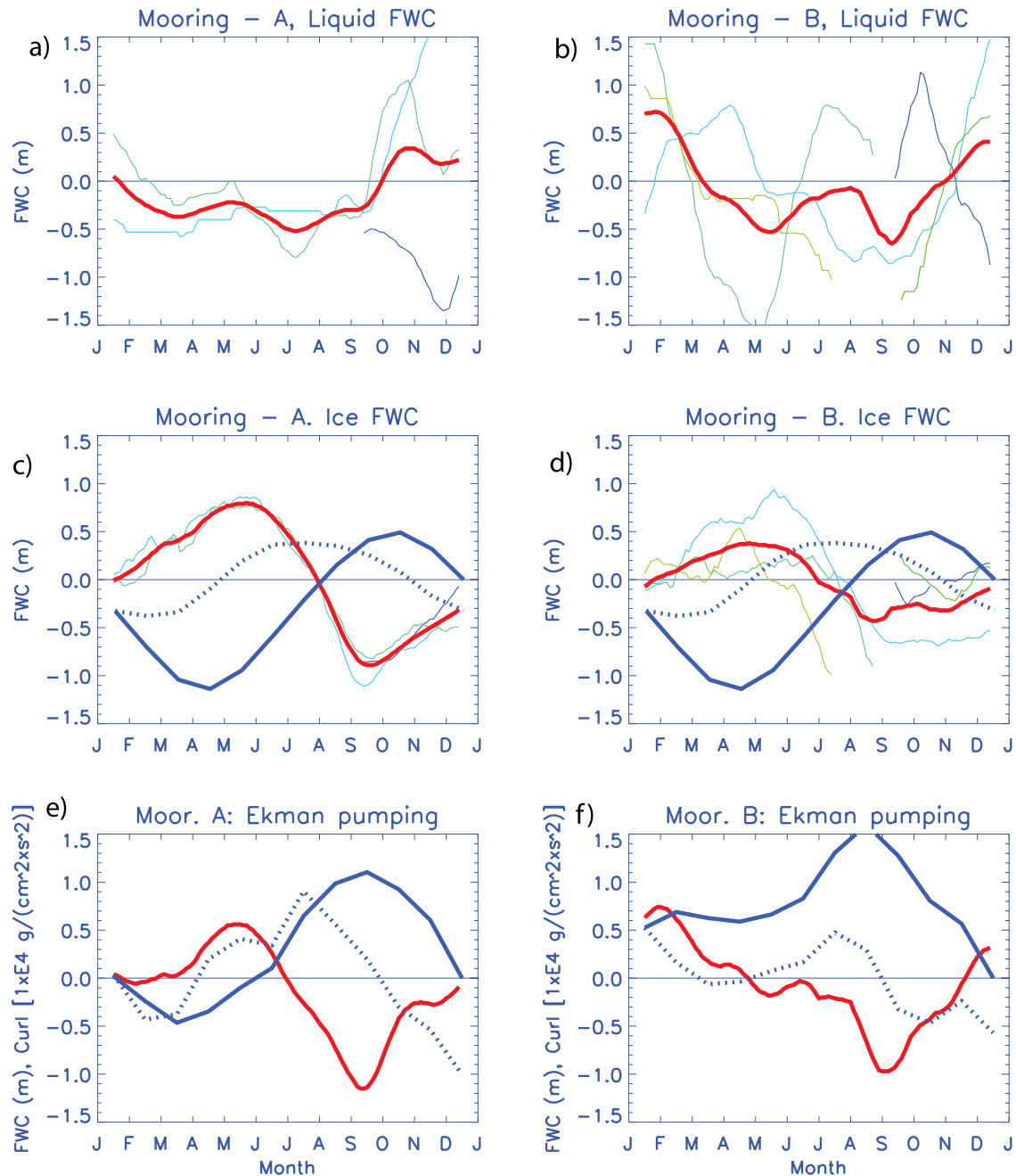
Figure 5. Mean annual seasonal cycles (red thick lines) of (a, b) liquid and (c, d) solid FWC component anomalies (m) and (e, f) anomalies of FWC due to Ekman pumping (red) at mooring A (Figures 5a, 5c, and 5e) and mooring B (Figures 5b, 5d, and 5f). Thin colored lines show seasonal changes for particular years (2003, deep blue; 2004–2005, light blue; 2005–2006, light green; 2007, dark green). Dotted and thick blue lines show anomalies of monthly air temperature (°C) and sum of degree days (°C) averaged for 2003–2007 over the BGR (Figures 5c and 5d). Note that the air temperature and sum of degree days are scaled with a factor of 0.025 to be compared with FWC values. In Figures 5e and 5f, blue dotted and solid lines depict seasonal anomalies of wind stress curl and sums of wind stress curl (similar to sums of degree days) averaged over a 300 × 300 km box centered at each mooring site.

maximum in July–August (minimum EP) and minimum in December–January (maximum EP); and the cumulative wind stress curl (solid blue line) indicates that the accumulation of freshwater in the BGR usually occurs between November and June (negative wind stress curl anomaly). Starting in June–July and until October–November the

wind stress curl does not support freshwater build up in the region and the BG can even release the freshwater because of the reduction or reversal of EP.

[37] On the other hand, the role of EP could be estimated from equation (4). Knowing anomalies of liquid (*FWCL*) and solid (*FWCI*) FWCs and assuming that other factors
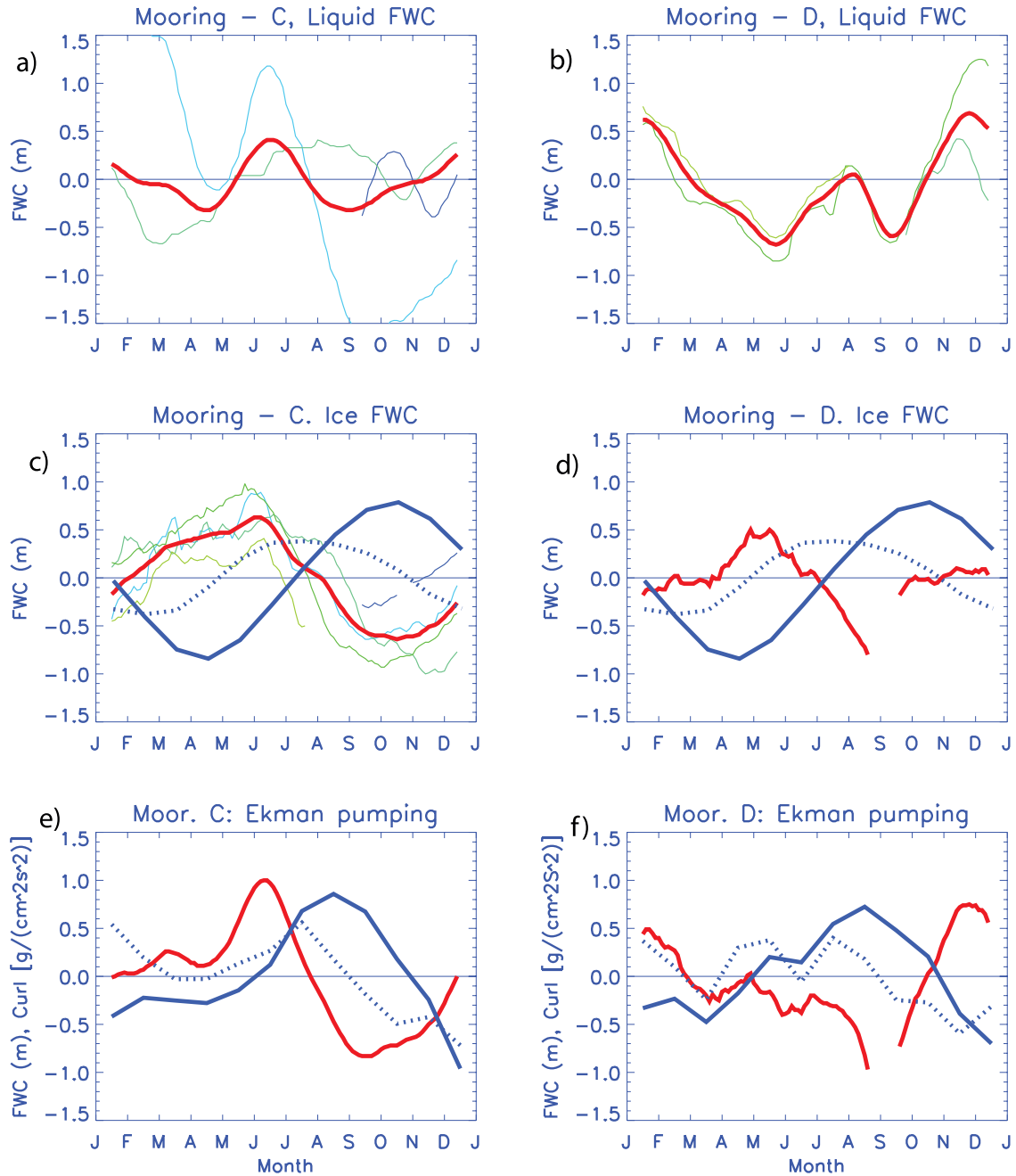
Figure 6. Same as in Figure 5 but for (a, c, e) mooring C and (b, d, f) mooring D.

(except EP) are already taken into account in *FWCE* or *FWCI* or are insignificant, the anomalies in EP can be expressed as a residual:

$$FWCE(t) = FWCL(t) - FWCI(t). \quad (5)$$

[38] These anomalies in liquid *FWCL* due to EP were calculated for each mooring and are shown in Figures 5e, 5f, 6e, and 6f (red line). One sees that these anomalies correlate well with the wind stress curl anomalies.

[39] On the basis of these results we surmise that the second maximum in BG FWC observed in summer (June–August, depending on mooring) is a result of interplay

between EP and freshwater changes due to sea ice seasonal transformations. The *FWCL* decreases from January to June–July because of a reduction in EP and because of sea ice formation and salt release. At this time both factors work together toward a reduction of *FWCL*. In June–July, sea ice starts melting and *FWCL* increases while EP is weakening or relatively stable and does not play an important role. In August, EP reaches its minimum or even becomes negative (i.e., forces upwelling in the central BGR resulting in relaxation of horizontal density/salinity gradients, weakening the BG anticyclonic circulation). Sea ice at this time melts but the rate of melting is decreasing. As a result, the EP effect (*FWCE*) dominates changes in *FWCI* (because of ice melt) and *FWCL* in the region reaches
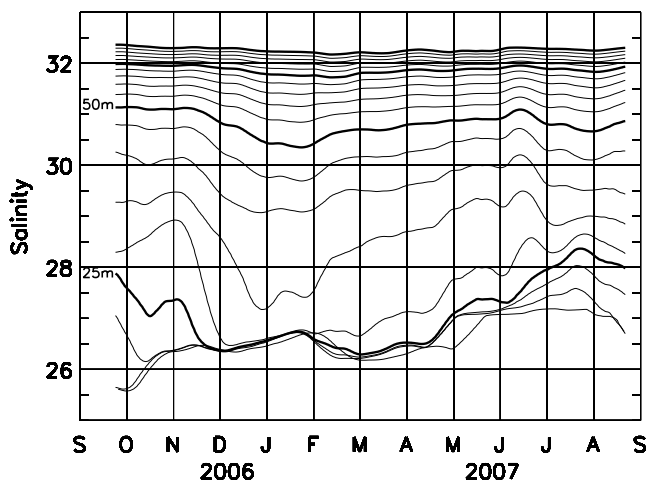
Figure 7. ITP-5 60-day running mean time series of water salinity at levels 10 dbar through 100 dbar with 5 dbar interval. Thick lines show 25 dbar (25 m) and 50 dbar (50 m) levels. In September and October the upper ocean layer is fresh. With time this layer mixes with deeper layers. By November the mixed layer depth reaches 30 m, and gradually its salinity increases because of mixing with deeper layers, ice growth, convection, and Ekman pumping. In July the upper ocean layer gets freshwater from ice melting, and the vertical ocean stratification increases.

its second minimum. In September, both factors contribute to the increase of *FWCL*: EP increases and sea ice continues melting but in October EP is the major influence on *FWCL* while sea ice starts growing reducing *FWCL*.

[40] These simple considerations demonstrate that the departure of the BG *FWCL* seasonal cycle from an ideal ice/ocean state is related to the wind forcing. Thus, the *FWCL* maximum observed in November–January (two to three months later than expected from thermodynamic sea ice transformations) is forced by the atmospheric anticyclonic circulation cell over the BGR.

[41] For a complete study of the seasonal variability of *FWCL*, it is important to analyze the potential for mixing between the upper and deep ocean layers as a mechanism that preserves freshwater in the BG. For example, Figure 7 demonstrates how the evolution of salinity and FWC in the BG can be influenced by (1) upper ocean transformations due to ice melt and growth, (2) EP, and (3) mixing. While surface salinity is more influenced by sea ice transformation and reaches a maximum in mid-January because of ice growth and salt release, salinity at deeper levels is controlled more by EP and exhibits minimum values in mid-January.

[42] In September and October the upper ocean layer is relatively fresh and the surface mixed layer quite thin (Figure 7). With time the surface layer deepens, entraining deeper layers and by November the mixed layer depth reaches 30 m. Gradually, the salinity of the surface layer increases because of ice growth and salt release, mixing with deeper layers. In July, the upper ocean layer again receives freshwater from sea ice melt and the vertical ocean stratification increases. In addition, because of Ekman

divergence, salinity anomalies generated by winter EP have to relax. In an ideal ocean without mixing, the freshwater content of the area remains the same after completing the EP seasonal cycle. In the real ocean, we speculate that because of mixing and entrainment of deeper layers the ocean can accumulate freshwater or salt and preserve it for long periods. Such preserved anomalies are strongly related to the mean anticyclonic baroclinic BG circulation.

3.3. Causes of Interannual FWC Changes in 2003–2007

[43] The small positive trends observed in 2003–2007 in the sea ice draft (Figure 4) apparently are the result of sea ice redistribution under wind forcing and are not influenced by the thermal regime, because the 2003–2007 air temperature linear trend averaged over the BGR is positive (0.72°C a^{-1}, not shown). Therefore, sea ice melt cannot contribute to the *FWCL* increase in the region at a rate of more than 100 cm a^{-1} (Figure 4, top). Geochemical water analysis in the BGR [*Carmack et al.*, 2008; *Alkire et al.*, 2009; *Guay et al.*, 2009] shows that the net effect of sea ice formation and melting removes ~30% of the freshwater contributed to this region by other sources. Therefore the only candidate responsible for this trend is EP, if we follow our conclusions about the mechanisms of *FWCL* changes in the BGR. Indeed, in 2003–2007 there was a significant trend in wind stress curl (Figure 8) with an unprecedented (for 1948–2008 period, see analysis of decadal changes in section 4) minimum of wind stress curl in 2007 when anticyclonic circulation dominated over all months including summer.

[44] In order to analyze interannual changes in the BGR *FWCL* volume we have used results from BG summer observations at repeat CTD and XCTD stations in conjunction with all other available mooring and drifter data from the cruise times (Figure 2). The *FWCL* was calculated for all years employing equation (1) for each T&S profile available in the region at this time. Then calculated FWCs were gridded using optimal analysis (section 2.2). While during 2003–2004 *FWCL* in the BGR showed little change (Figure 9), in 2005 the total *FWCL* in the region began to increase, reaching 20,000 km³ in 2007. The maximum annual trend of *FWCL* accumulation was observed at the new center of the BG (which was first established in the 1990s, see section 4) with a rate of approximately 1.5 m a^{-1} in the center and tapering away with increasing radius (Figure 10). Preliminary data from the BGOS 2008 cruise indicate that the *FWCL* in the BG continued to rise in 2008 and reached 21,000 km³, a historical maximum from all available years of observations. Compared to 1970s climatology (the pre-1990s decade with the most extensive data coverage, Figure 1) there has been a *FWCL* increase in the BG of approximately 5000 km³. This is comparable with the volume of freshwater annually delivered to the Arctic Ocean by rivers and through Bering Strait (5700 km³ a^{-1} [*Serreze et al.*, 2006]).

[45] Both the mooring (Figure 4) and ITP data (Figure 11) demonstrate that from 2003 to 2007 the absolute maximum of FWC was located in the southeast region of the BG (near the location of mooring D). The maximum rate of *FWCL* increase over this time period (178 cm a^{-1}) (Figure 4) is observed at mooring B; somewhat smaller rates are observed at moorings A and C. Summer CTD data further
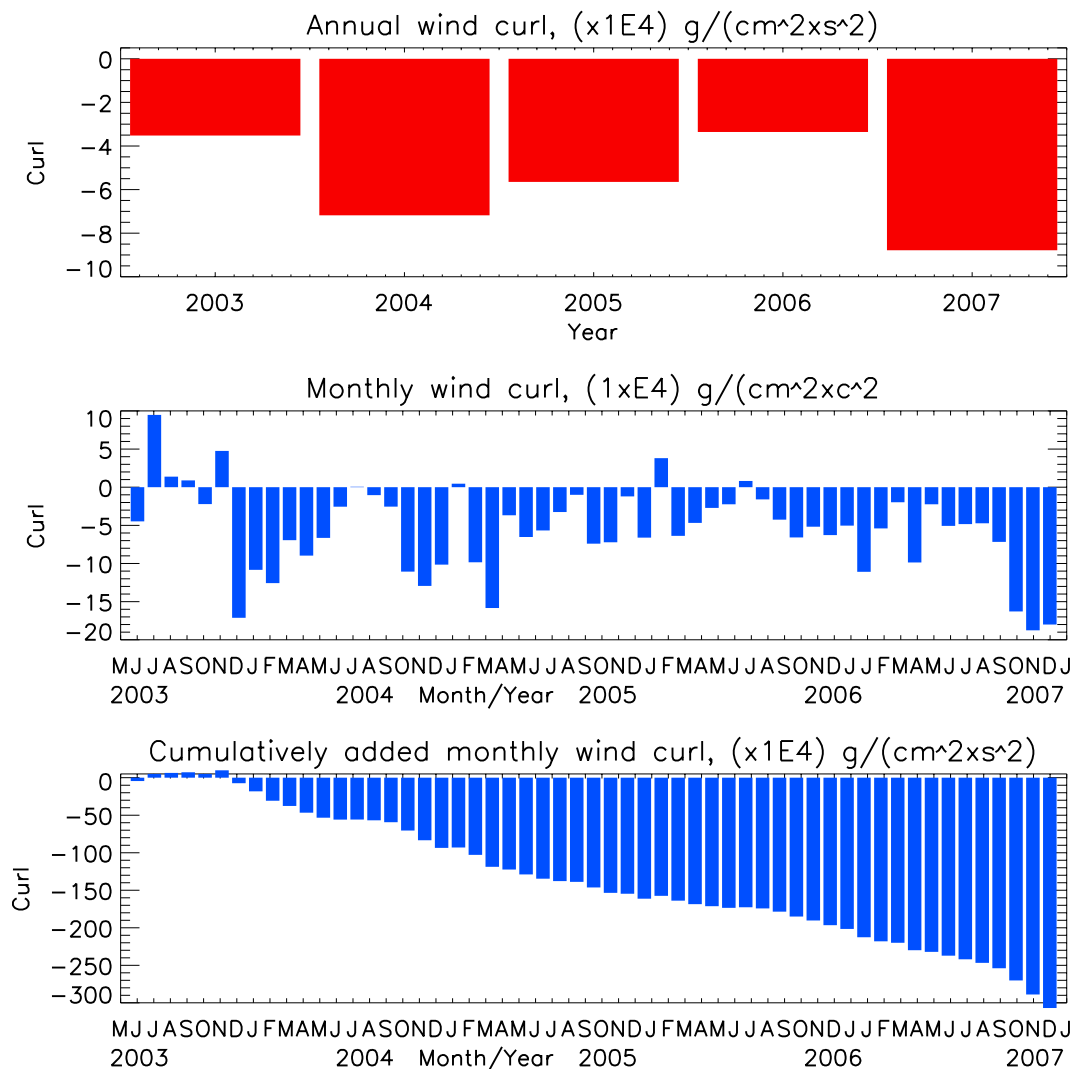
Figure 8. Wind curl time series over the BGR showing (top) annual, (middle) monthly, and (bottom) integrated in time.

indicate that this trend could be as high as $140-150$ cm a^{-1} in places (Figure 10). The regional differences in trends can be explained by regional differences in the EP (atmospheric circulation). Figure 12 shows annual SLPs and geostrophic winds for 2003–2007 where centers of the atmospheric circulation (max/min EP) and their intensity can be easily identified. On the basis of Figure 12, the largest EP should be observed in 2004, 2005 and 2007 which is in agreement with wind stress curl data shown in Figure 8.

[46] Moorings B and C have no overall *FWCL* increase between 2003 and 2004 or even a small reduction (Figure 4). This could be due to a reduced annual wind curl in 2003 (Figure 8; note also the monthly wind curl is positive in June, July, August, and October) with a low-gradient SLP field (Figure 12). In 2004–2005, SLP gradients intensified and the absolute wind curl over the region (Figure 8) increased by approximately 30% relative to the previous year and the region influenced by anticyclonic winds extended over the entire Canada Basin (Figure 12). In 2004, the center of circulation and maximum EP was very

close to mooring B, accounting for the significant increase of FWC at this mooring by December of 2004 (4 and Figures 3b). Moorings A and C also show accumulation of freshwater during this period but at a lower rate (Figures 3a, 3c, and 4). In 2005–2006, the SLP gradients in the region relaxed, absolute wind curl decreased by approximately 35% and the freshwater accumulation at all moorings fell accordingly. Another jump in the FWC was observed in 2007 (Figures 3, 4, and 8) when an anomalous anticyclonic circulation regime dominated the Arctic Basin for the entire year (Figure 12) and the annual wind curl reached its absolute minima in the 2000s (Figure 8).

4. Decadal Shift

[47] On the basis of our analysis of the decadal distributions of *FWCL* in the BGR (Figure 13), decadal distributions of SLP fields (Figure 14) and decadal changes of wind stress curl (Figure 15), we conclude that the anticyclonic atmospheric circulation dominated over the BG since at
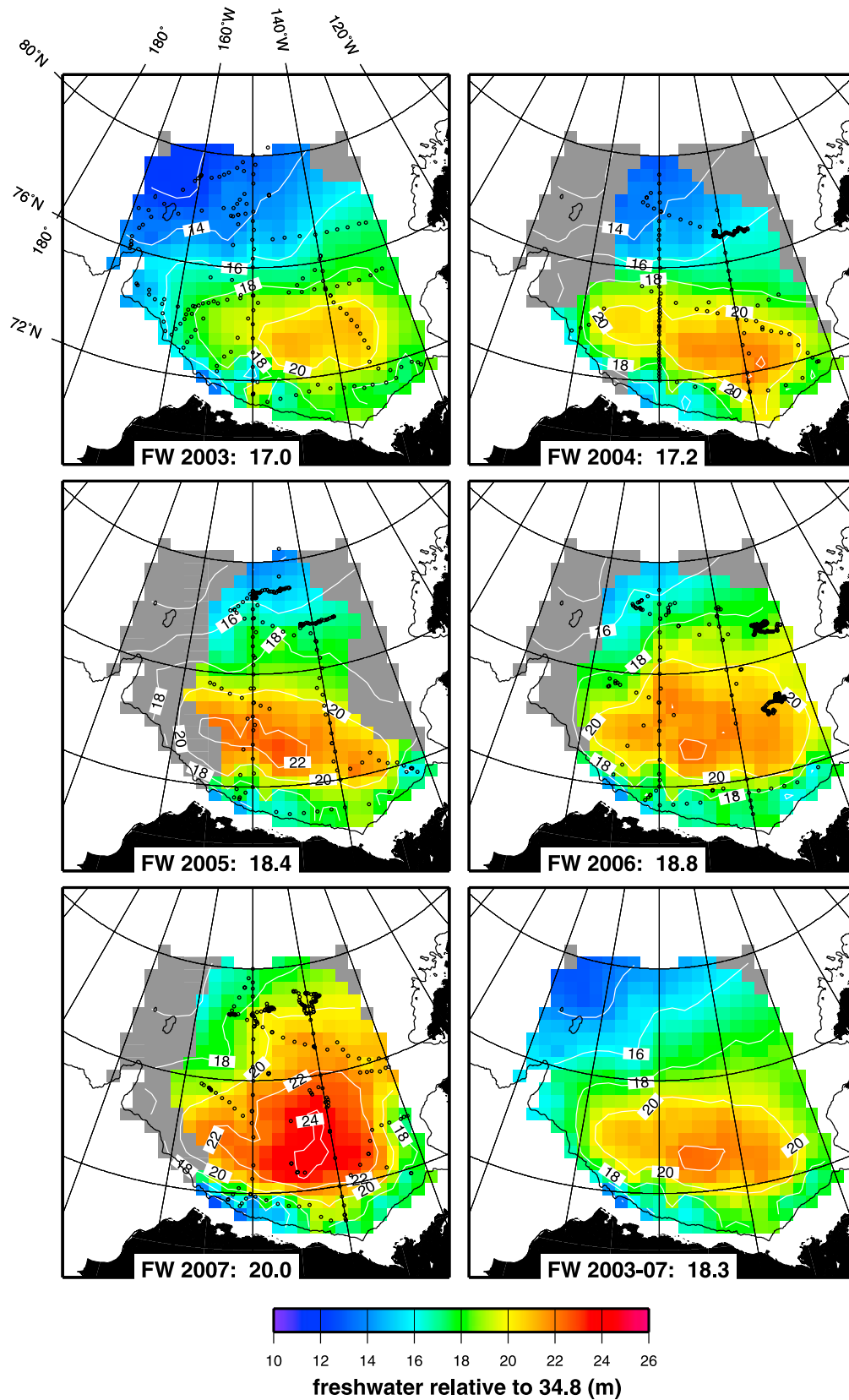
Figure 9. Late summer FWCL distribution characteristics. Colors and contours show BGR FWCL (m) relative to salinity 34.8. Black numbers in white boxes show regional summer FWC volume (km³) for each year. Black dots show locations of CTD data used for the analysis. Gray-colored pixels depict areas where FWCL error of interpolation exceeds 2 m.
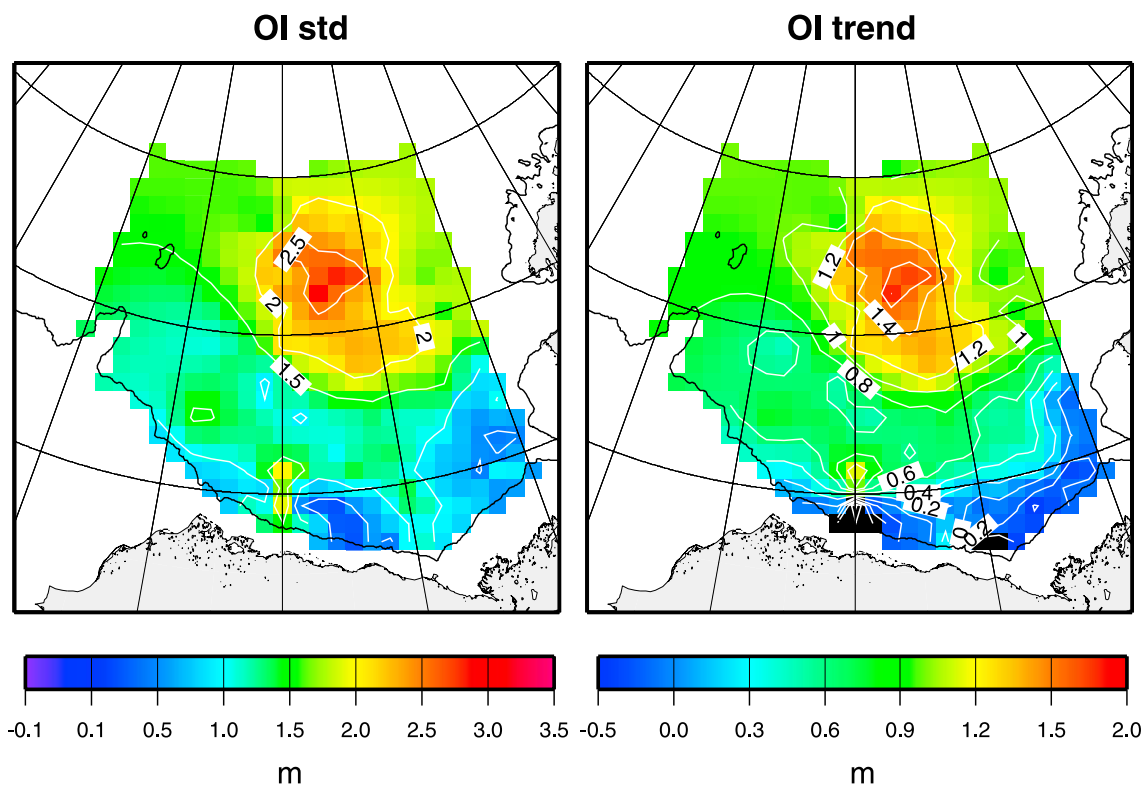
Figure 10. (right) FWCL trend (m a^{-1}) for 2003–2007 in the BGR based on results of optimal interpolation (OI). (left) Standard deviations (m).

least the 1950s enabling freshwater accumulation in this region of the Arctic Ocean (via negative wind curl and consequently positive EP). The rate of freshwater accumulation changes from decade to decade (Figure 13) and the center of the FWC maximum also changes depending on the atmospheric conditions (e.g., location of the Arctic High) (Figure 14). We speculate that fresh water characteristics in the BG depend on three parameters: surface layer characteristics of the regions which supply this fresh water in the BG, strength of the wind curl, and a location of the Arctic High center. Indeed, the historical hydrographic data indicate that FWCL in the BGR did not change significantly from decade to decade in the 1950–1980s period (Figure 13) which is in agreement with decadal SLP fields and position of the Arctic High. Wind stress curl (Figure 15) also did not change significantly during the 1960–1980s. Note that the information about wind stress curl (Figure 15) and information about location of the Arctic High center have to be analyzed together to explain changes in FWCL and its center of maximum. For example, the wind stress curl values over the region in the 1960s and 1970s are practically identical but the center of the Arctic High shifted westward in the 1970s (Figure 14) and the center of the BG maximum of FWCL also shifted to the new position. It is also important to remember that the FWCL distribution for the 1970s is more accurate than for other pre-1990s decades because the hydrographic data coverage in the 1970s was relatively good [see *Timokhov and Tanis*, 1997, 1998] and therefore the FWCL from the 1970s may be used as a climatologic benchmark characterizing all pre-1990s conditions.

[48] The SLP (Figure 14) and FWCL (Figure 13) conditions in the 1990s differed significantly from the pre-1990s climatologic conditions: the maximum of the FWCL distribution shifted to the southeast and increased in magnitude. The spatially integrated BG FWCL for the 1990s exceeded the climatologic mean for the 1950–1980 by approximately 1400 km^3; lateral gradients of FWCL increased as well. Thus, in the 1990s the freshwater reservoir of the 1950–1980s with its center at 76°N and 150°W "released" its freshwater which was relocated into a new center with coordinates 73.5°N and 143°W. We also conclude that the major cause of this relocation was the change in the atmospheric circulation, intensity and center of the maximum EP. While the EP in the BG "traditional" region shown in Figure 1 decreased, the center of EP shifted southward and eastward (Figure 14) and reorganized the FWCL fields respectively. As a result the BG freshwater reservoir contracted but intensified. Unfortunately, the hydrographic data from the 1990s are very sparse in the eastern half of the BGR so that we are unable to positively determine the BG FWCL maximum center precisely in the 1990s. But the information from the western half of the BG is good and indicates that there was a substantial decrease in FWCL in this region relative to pre-1990s (Figure 13), confirming at least partially our conclusion about FWCL center relocation in the 1990s.

[49] In the 2000s, the "decadal" (based on 2000–2007 data) volume of liquid freshwater in the BG is comparable to what it was in the 1990s. This is because some data from 2000 to 2002 showed some reduction in the BGR FWCL. The FWCL increase in 2003–2007 is consistent with wind
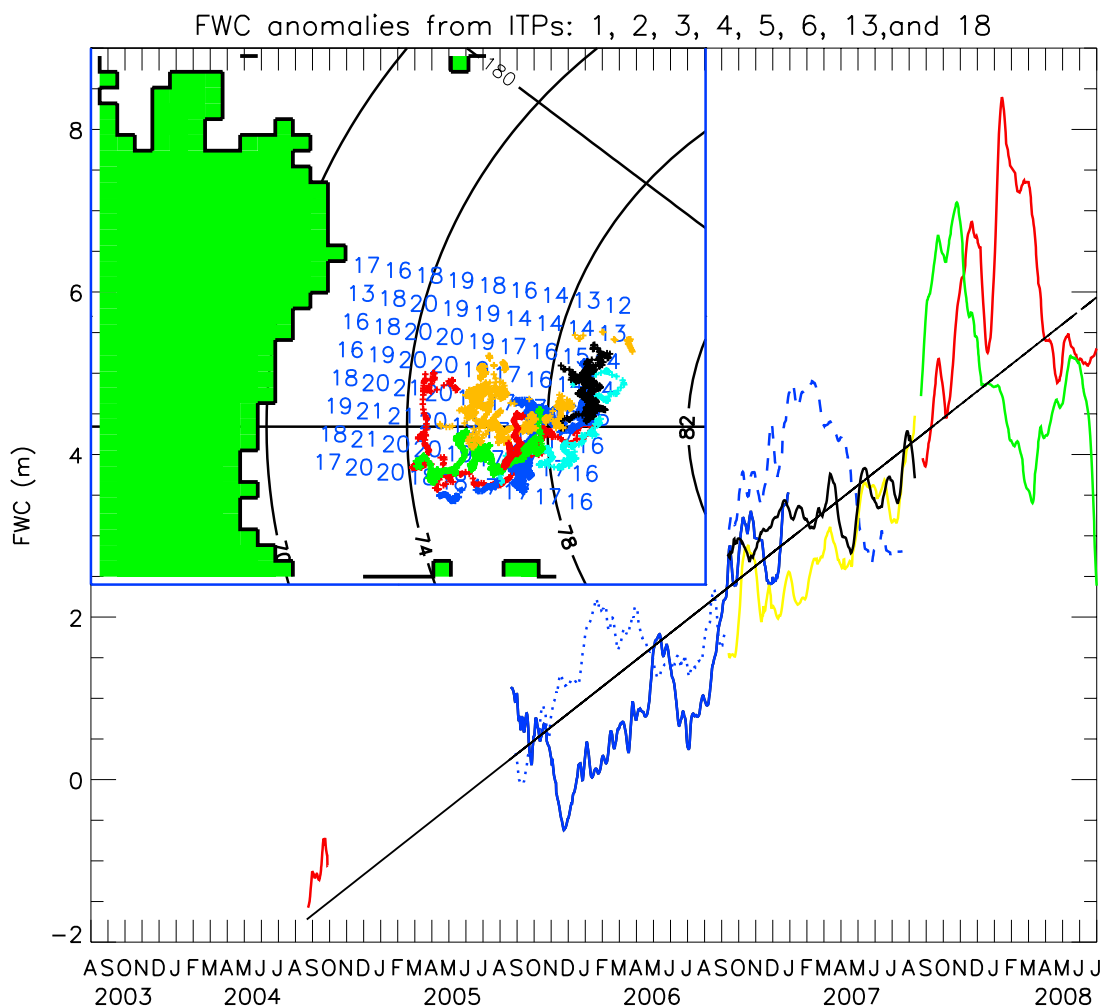
Figure 11. FWCL content anomalies (m) calculated on the basis of ITP data relative to 2003–2006 mean FWCL distribution for the region (numerals in inset). Colored lines show different ITP FWCL time series. The black solid line depicts the overall linear trend calculated using all ITP data (193 cm a^{-1}). The inset shows ITP trajectories and the mean gridded values.

stress curl dynamics (Figure 15) and the SLP distribution for the 2000s (Figure 14). Except for 2000–2002, in the 2000s, the Arctic High was perfectly located over the BGR, centered over mooring B (where the maximum trend in *FWCL* accumulation was observed) and the wind stress curl reached its historical minimum (maximum EP) (Figure 15).

[50] Summer time series of FWC in different vertical layers of the BG, including sea ice, shows that the maximum change occurred in the mixed layer (as expected) and that in the 1990s the FWC in the mixed layer increased by 2400 km^3 (Table 1) relative to the 1980s. The volumes of freshwater in summer and winter Pacific Water decreased. Volumetric changes of freshwater in the Atlantic Water layer for the same period are small relative to the accuracy of the estimates (150 km^3). Small increase in *FWCL* in the mixed layer and reduction in the Pacific layer relative to the 1990s were observed in the 2000s (Table 1).

[51] Our explanations for decadal variability of FWC in the BGR are speculative, but it is clear that the BG *FWCL* field in the 2000s is not in steady state despite the more than

10 years of prevailing anticyclonic atmospheric circulation (1997–2007). There are strong increasing trends in BG FWC in 2003–2007 observed at the mooring locations, along ITP trajectories and at the standard summer shipboard BGOS CTD station sites. We speculate and provide some observational evidence that there are three major causes of these changes, namely, (1) wind-generated EP which represents the mechanical part of the ocean freshwater redistribution, (2) mixing and changes of water stratification, and (3) sea ice transformations accompanied by freshwater and salt release. More quantitative analysis of these processes has to be done by means of numerical modeling: a subject for future studies.

5. Conclusions

[52] Summarizing the major results of this study, we conclude the following.

[53] 1. The Beaufort Gyre in the southern half of the Canada Basin is the largest freshwater reservoir of the
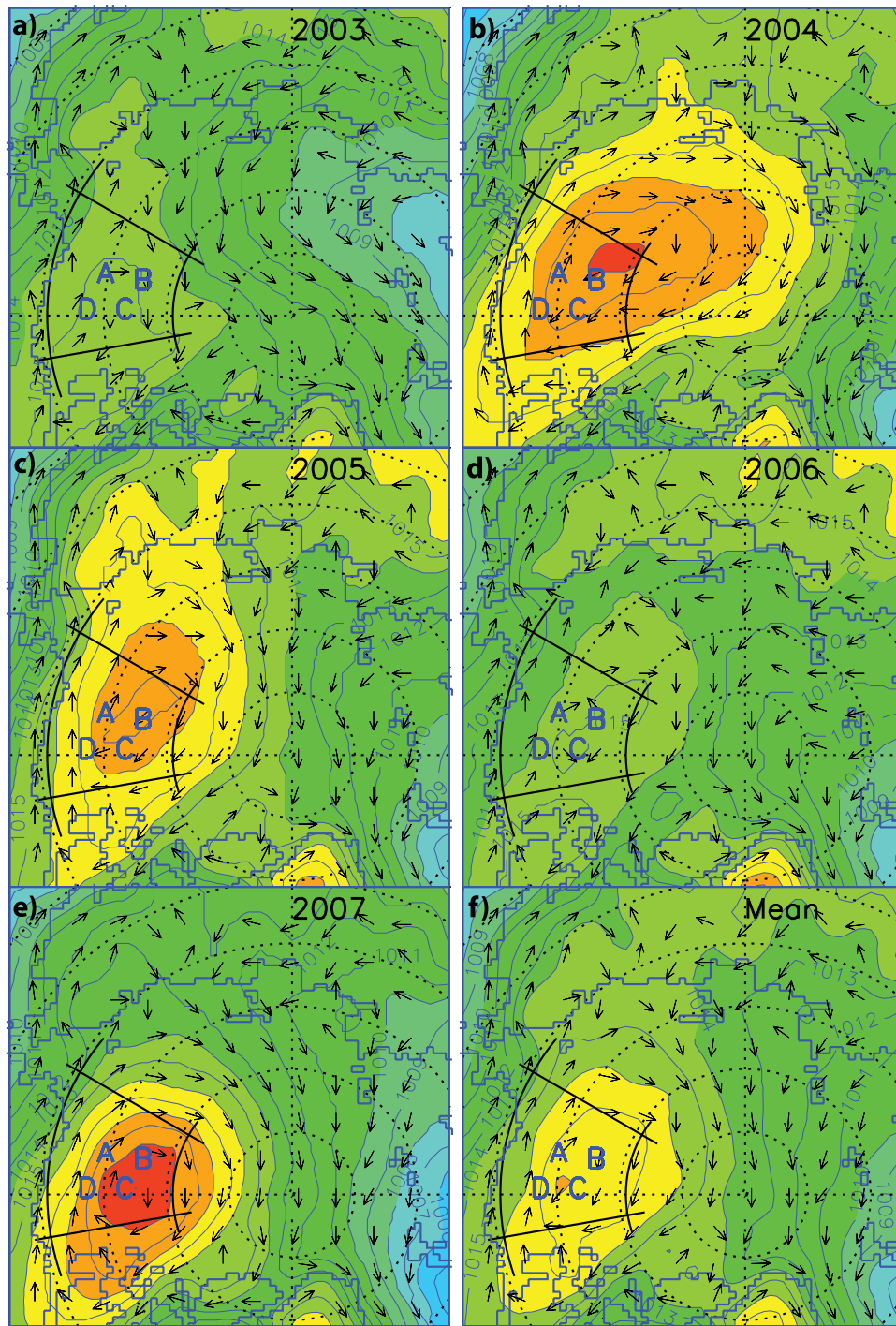
Figure 12. (a, b, c, d, e) Annual SLP (hPa) (solid contours and colors) and geostrophic wind direction (vectors) in 2003–2007. A, B, C, and D depict mooring locations, and black lines bound the BG Region. (f) SLP and wind direction averaged for 2003–2007. It is expected that largest Ekman pumping should be observed in 2004, 2005, and 2007, which is in agreement with Figure 8.

Arctic Ocean. It contains approximately 20,000 km^3 of liquid and approximately 800 km^3 of solid (sea ice) freshwater (on the basis of a mean ice thickness in the region of 2.0 m). Decadal, interannual and seasonal changes in total FWC influence the extent of sea ice cover, the surface albedo, the energy balance, the temperature and salinity structure of the water masses, and biological processes in the entire Arctic Ocean. Moreover, the intensity of the Atlantic Ocean Meridional Overturning Circulation can be influenced significantly by freshwater fluxes from the Arctic Ocean. Our results demonstrate that the seasonal changes in BG total FWC range from 5% to 10% of its total
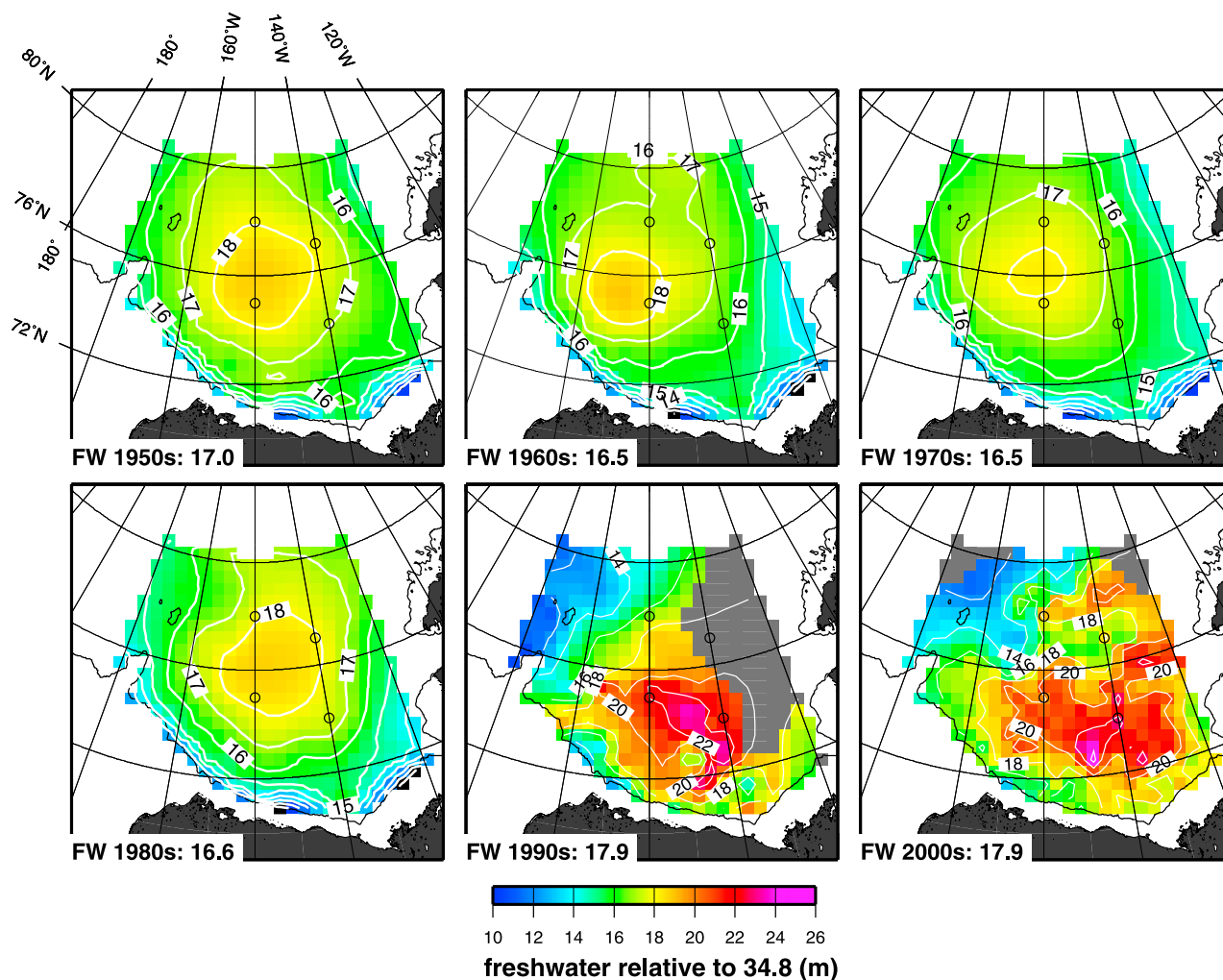
Figure 13. Contour plots of decadal summer FWCL (m) in the BG relative to salinity 34.8. The summer FWCL volume estimates for the BG region (1000 km³) for each decade are indicated by black numbers in white boxes. Data for 1950–1980 are from summer gridded fields [*Timokhov and Tanis*, 1997, 1998]. The 1990 and 2000 data are optimally interpolated fields from observations acquired during the summer period for each decade. Gray shading indicates expected error in the interpolation is greater than 2 m. Black dots show locations of BGOS mooring locations for reference.

volume depending on the intensity and sense of the atmospheric circulation. Interannual changes based on the data from 2003 to 2008 can reach as much as 1000 km³ a⁻¹. The decadal change range is approximately 1000 km³ per decade prior to 2000, but has accelerated since 2003. This estimate of decadal timescale variability is likely a lower bound since it is based on climatologic fields for calendar decades (1950s, 1960s, 1970s, 1980s, 1990s, and 2000s) which do not coincide with the timing of climatic circulation regimes (cyclonic and anticyclonic [*Proshutinsky and Johnson*, 1997; *P*2002]). We speculate on the basis of our calculation of wind stress curl (Figure 15, bottom) that the differences in *FWCL* between cyclonic and anticyclonic circulation regimes are significantly larger than the decadal changes recorded by *Timokhov and Tanis* [1997, 1998].

[54] 2. On the basis of the admittedly flawed decadally averaged climatologies, BG FWC appeared to be relatively stable between the 1950s and 1980s. However, the 1990s conditions differ significantly from the pre-1990s climatologic conditions: the center of the FWC maximum shifted to the southwest and appeared to contract in area. In spite of the areal reduction, the spatially integrated BG FWC increased by approximately 1400 km³ relative to the earlier climatology, while lateral gradients of FWC increased. We speculate that under these conditions, the BG geostrophic circulation spun up and the baroclinic part of the Transpolar Drift current intensified and shifted toward Canada, accelerating sea ice drift and redistributing sea ice in this region.

[55] 3. We speculate and provide some observational evidence that there are three major causes of the FWC changes observed in the BG at different timescales, namely, (1) wind-generated EP which represents the mechanical part of the ocean freshwater redistribution, (2) mixing and changes of water stratification, and (3) sea ice transformations accompanied by the release of freshwater and salt.
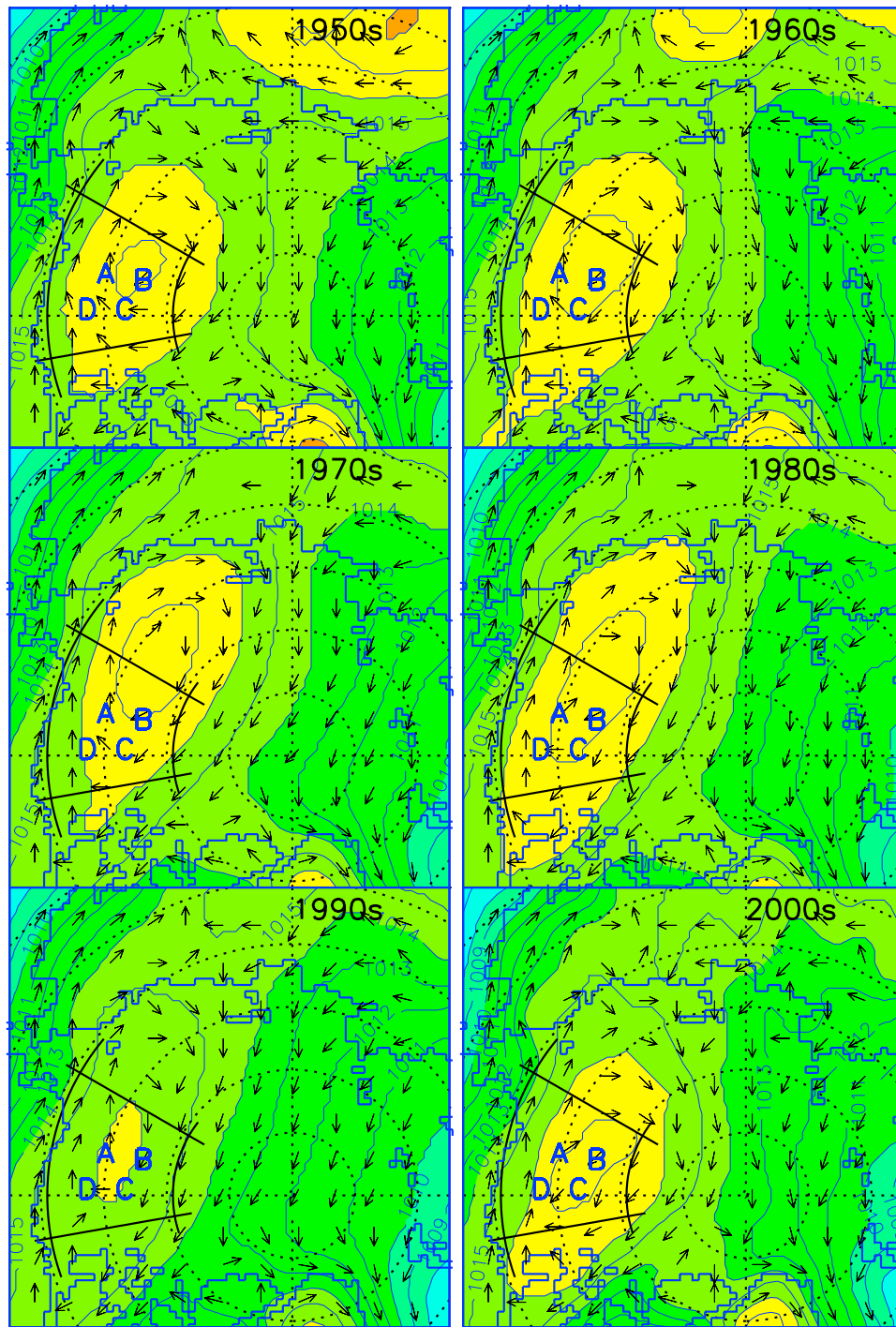
Figure 14. Annual SLP (hPa) (solid contours and colors) and geostrophic wind direction (vectors) in 1950s through 2000s. A, B, C, and D depict mooring locations, and black lines bound the BG Region. In 1990s, the Arctic High shifted southeast, and this explains relocation of the center of FWCL accumulation observed in 1990s (Figure 13).

[56]   4. The major cause of the large *FWCL* in the BGR is the process of EP generated by the climatologic anticyclonic atmospheric circulation over the Canada Basin with a center in the Beaufort Gyre. Our observational data analysis confirms this hypothesis formulated by *P*2002. Mechanically, the seasonal variability of *FWCL* follows wind curl changes with a maximum in November–January and a minimum in June–August depending on changes in atmospheric circulation. The atmospheric and oceanic thermal regimes regulate seasonal transformations of *FWCL* because of the seasonal cycle of sea ice melt and growth. The seasonal *FWCL* in the Beaufort Gyre has two pronounced
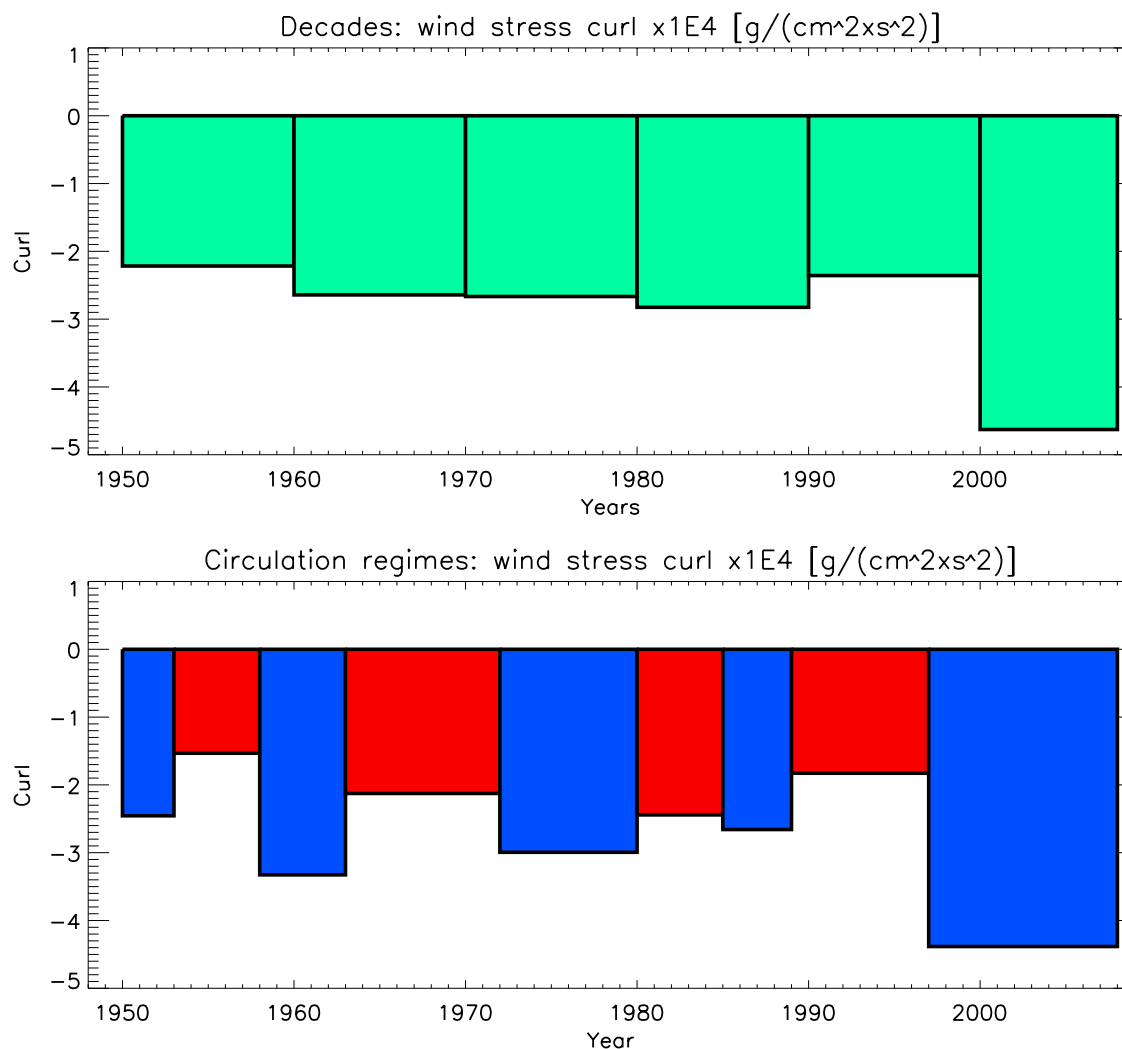
Figure 15. (top) Wind stress curl ($\times 10^4$ g cm^{-2} s^{-2}) averaged for decades and (bottom) circulation regimes over the BG Region. In Figure 15 (bottom) periods of anticyclonic circulation regimes are shown as blue bars, and cyclonic regimes are shown as red ones.

peaks shifted by approximately six months. The first (small) peak (June–August depending on mooring) is observed when the sea ice thickness reaches its minimum (maximum freshwater release from sea ice to the ocean) and when EP is very close to its minimum (maximum wind curl). The second maximum (large) is observed in November–January when wind curl reaches its minimum (maximum EP) and the salt flux from the growing sea ice has not reached its maximum.

[57]   5. The conventional practice for measuring the Arctic Ocean hydrography (sampling in fall when the Arctic is accessible by research icebreakers when sea ice coverage is minimum and by aircraft in spring when sea ice is suffi- ciently strong and daylight is longer) misses natural sea- sonal variability and underestimates seasonal variability of hydrographic fields, their gradients, and circulation patterns. Note that the seasonal Polar Science Center Climatology [Steele et al., 2001] which is based on observations made in August–September or March–April [see Timokhov and

Tanis, 1997, 1998] should be used with caution because it does not fully capture the seasonal variability of salinity in the upper 300 m of the water column.

[58]   6. The interannual changes in the BG were estimated on the basis of 2003–2008 observations of the BG hydrog- raphy at standard sections repeated annually, and also using moorings and ITPs which provided year-round T&S high vertical resolution data. Both the mooring and ITP data

Table 1. Freshwater Content in the Beaufort Gyre Region Relative to Salinity 34.8[a]

Decade/Layer	Salinity	1970s	1980s	1990s	2000s
Mixed layer	S < 31	4.2	4.9	7.3	7.5
Summer Pacific	31 < S < 33	8.5	8.0	7.1	6.6
Winter Pacific	33 < S < 34	2.7	2.7	2.2	2.1
Deeper layers	S > 34	1.1	1.1	1.1	1.1
Total		16.5	16.6	17.7	17.3

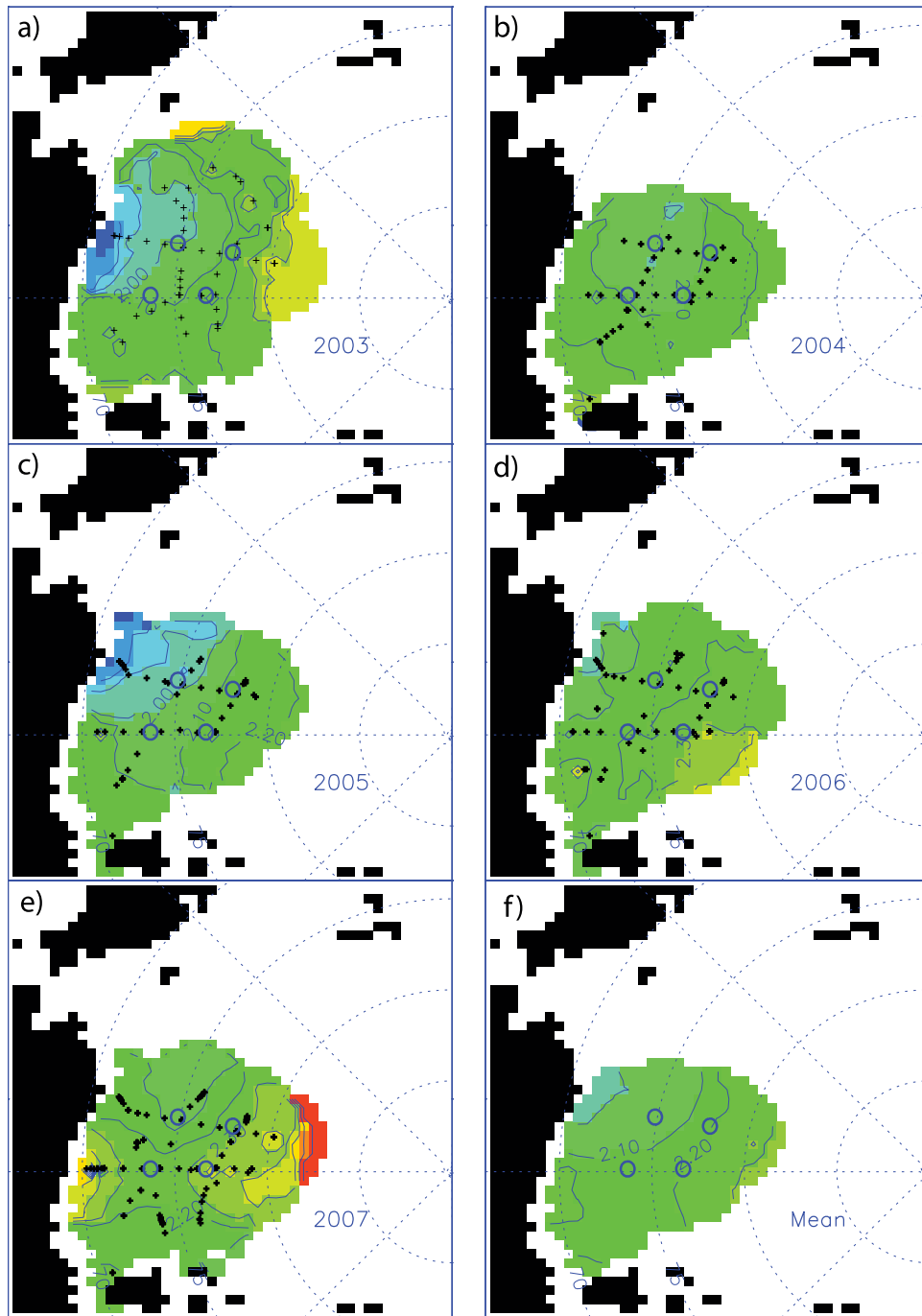[a]Freshwater content is shown in 10^3 km^3.

Figure A1. (a, b, c, d, e) FWCL coefficients (ratio of FWCL from sea surface to the level of salinity 34.8 and FWCL from 65 m to the level of salinity 34.8) calculated from summer CTD surveys for each year from 2003 to 2007. (f) The 2003–2007 mean. Open blue circles depict locations of BGOS moorings A (75°N, 150°W), B (78°N, 150°W), C (77°N, 140°W), and D (74°N, 140°W).

demonstrate that the BG FWC field is in transition; the processes of FWC accumulation and release are not in balance. There are strong FWC positive trends in the 2003–2007 pentade at the mooring sites, along ITP trajectories, and at the standard BGOS summer shipboard CTD measurement sites. The maximum FWC trend of 178 cm a^{-1} for this period was observed at 78°N and 150°W while the FWC increased at a smaller rate at moorings A, C, and

D. Preliminary analysis of our 2008 data shows that the FWC in the BGR is continuing to increase.

Appendix A: Reconstruction of Mooring and ITP FWC Data to Take Into Account the Upper Ocean Layers

[59] In order to investigate the full-scale FWC variability (including the upper layers of the ocean which were not

covered by observations during the entire year) at each mooring location, we have reconstructed these data by a simple regression of FWC calculated from the shipboard CTDs, including those taken at each mooring site during deployment and recovery operations. In this procedure, we used CTD data to determine a ratio between FWC calculated for the entire water column (from the surface to the depth of the 34.8 isohaline) and for the column from 65 m or 95 m down to the 34.8 isohaline. These summer coefficients for 2003–2007 are relatively stable, both spatially and temporally (Figure A1).

[60] Since 2004, a significant amount of T&S data have become available from Ice-Tethered Profilers (ITPs: http://www.whoi.edu/itp). ITP profiles cover depths between 7 and 760 m, capturing the surface mixed layer in winter but missing the thin, very fresh waters just below the ice that can occur in summer. In order to better reconstruct the seasonal cycle of FWC change at moorings, we have made calculations on the basis of ITP data to investigate how the FWC ratio changes during the course of a seasonal cycle. The FWC in the upper 8 m (shallower than the top of the ITP profile) were calculated assuming that the salinity at 8 m extends to the ocean surface. This approach works very well for at least nine months of the year when the upper mixed layer extends below 8 m. During ice melt season (June–August) this procedure underestimates the amount of FWC in the water column by approximately 0.15–0.20 m. This is the difference between FWC calculated by multiplying the FWC below 8 m by a ratio coefficient between FWC calculated for the entire water column (from the surface to the 34.8 isohaline) and FWC calculated for the column from 8 m down to the 34.8 isohaline using summer CTD data. This ratio is very stable and is around 1.1 and results in the underestimation of FWC from ITPs by approximately 10% of the total FWC in the water column in summer (not shown).

[61] ITP FWC anomalies for Figure 11 are calculated relative to a reference surface on the basis of the 2003 to 2006 summer BGOS CTD stations. The ITP FWC is computed as described in the text above. Unlike the other maps presented in this paper, a polynomial surface was fit to the CTD station data to produce the gridded surface at 50 km spacing (as in the paper by *Carmack et al.* [2008]). The anomalies at each time are the ITP FWC value subtracted from the corresponding grid value.

References

Aagaard, K., and E. C. Carmack (1989), The role of sea ice and freshwater in the Arctic circulation, *J. Geophys. Res.*, *94*, 14,485–14,498, doi:10.1029/JC094iC10p14485.

Aagaard, K., and L. Coachman (1975), Toward an ice free Arctic Ocean, *Eos Trans. AGU*, *56*(7), 484–486.

Aagaard, K., and P. Greisman (1975), Towards new volume and heat budgets for the Arctic Ocean, *J. Geophys. Res.*, *80*, 3821–3827, doi:10.1029/JC080i027p03821.

Aagaard, K., J. H. Swift, and E. C. Carmack (1985), Thermohaline circulation in the Arctic Mediterranean seas, *J. Geophys. Res.*, *90*, 4833–4846, doi:10.1029/JC090iC03p04833.

Alkire, M. B., K. K. Falkner, R. W. Collier, J. Morison, and C. K. Guay (2009), River runoff is the dominant source of freshwater to the central Arctic Ocean and Beaufort Sea during spring 2008, *Eos Trans. AGU*, *89*(53), Fall Meet. Suppl., Abstract C51A–0523.

Belkin, I. M., S. Levitus, J. Antonov, and S.-A. Malmberg (1998), "Great salinity anomalies" in the North Atlantic, *Prog. Oceanogr.*, *41*, 1–68.

Bretherton, F. P., R. E. Davis, and C. B. Fandry (1976), A technique for objective analysis and design of oceanographic experiments applied to MODE-73, *Deep Sea Res. Oceanogr. Abstr.*, *23*, 559–582.

Budyko, M. I. (1969), The effect of solar radiation variations on the climate of the Earth, *Tellus*, *21*, 611–619.

Carmack, E. C. (2000), The Arctic Ocean's freshwater budget: Sources, storage and export, in *The Freshwater Budget of the Arctic Ocean*, *NATO Sci. Ser.*, vol. 2, edited by E. L. Lewis, pp. 91–126, Kluwer Acad., Dordrecht, Netherlands.

Carmack, E., F. McLaughlin, M. Yamamoto-Kawai, M. Itoh, K. Shimada, R. Krishfield, and A. Proshutinsky (2008), Freshwater storage in the Northern Ocean and the special role of the Beaufort Gyre, in *Arctic-Subarctic Ocean Fluxes: Defining the Role of the Northern Seas in Climate*, edited by R. R. Dickson, J. Meincke, and P. Rhines, pp. 145–170, Springer, New York.

Clarke, R. A., and J. C. Gascard (1983), The formation of Labrador Sea water. Part I: Large-scale processes, *J. Phys. Oceanogr.*, *13*, 1764–1778, doi:10.1175/1520-0485(1983)013<1764:TFOLSW>2.0.CO;2.

Coachman, L. K., and K. Aagaard (1974), Physical oceanography of Arctic and sun-Arctic seas, in *Arctic Geology and Oceanography*, pp. 1–72, Springer, New York.

Comiso, J. (1999), Bootstrap sea ice concentrations from NIMBUS-7 SMMR and DMSP SSM/I, http://nsidc.org/data/nsidc/0079.html, Natl. Snow and Ice Data Cent., Boulder, Colo., (Updated 2008).

Curry, R., and C. Mauritzen (2005), Dilution of the northern North Atlantic Ocean in recent decades, *Science*, *308*, 1772–1774, doi:10.1126/science.1109477.

Delworth, T., S. Manabe, and R. J. Stouffer (1993), Interdecadal variations of the thermohaline circulation in a coupled ocean-atmosphere model, *J. Clim.*, *6*, 1993–2011, doi:10.1175/1520-0442(1993)006<1993:IVOTTC>2.0.CO;2.

Delworth, T., S. Manabe, and R. J. Stouffer (1997), Multidecadal climate variability in the Greenland Sea and surrounding regions: A coupled model simulation, *Geophys. Res. Lett.*, *24*, 257–260, doi:10.1029/96GL03927.

Dickson, R., J. Meincke, S. A. Malmberg, and A. J. Lee (1988), The great salinity anomaly in the northern North Atlantic, *Prog. Oceanogr.*, *20*, 103–151, doi:10.1016/0079-6611(88)90049-3.

Dickson, R. R., J. Meincke, and P. Rhines (2008), A general introduction, in *Arctic-Subarctic Ocean Fluxes: Defining the Role of the Northern Seas in Climate*, chap. 1, pp. 1–12, Springer, New York.

Dukhovskoy, D. S., M. A. Johnson, and A. Proshutinsky (2004), Arctic decadal variability: An auto-oscillatory system of heat and freshwater exchange, *Geophys. Res. Lett.*, *31*, L03302, doi:10.1029/2003GL019023.

Dukhovskoy, D., M. Johnson, and A. Proshutinsky (2006), Arctic decadal variability from an idealized atmosphere-ice-ocean model: 2. Simulation of decadal oscillations, *J. Geophys. Res.*, *111*, C06029, doi:10.1029/2004JC002820.

Emery, W. J., and R. E. Thomson (1997), *Data Analysis Methods in Physical Oceanography*, 634 pp., Elsevier Sci., New York.

Fowler, C. (2003), Polar Pathfinder daily 25 km EASE-grid sea ice motion vectors, http://nsidc.org/data/nsidc-0116.html, Natl. Snow and Ice Data Cent., Boulder, Colo. (Updated 2007.)

Gandin, L. S. (1965), *Objective Analysis of Meteorological Fields*, Isr. Program for Sci. Transl., Jerusalem.

Guay, C. K. H., F. A. McLaughlin, and M. Yamamoto-Kawai (2009), Differentiating fluvial components of upper Canada Basin waters based on measurements of dissolved barium combined with other physical and chemical tracers, *J. Geophys. Res.*, *114*, C00A09, doi:10.1029/2008JC005099.

Hakkinen, S. (1993), An Arctic source for the great salinity anomaly: A simulation of the Arctic ice–ocean system for 1955–1975, *J. Geophys. Res.*, *98*, 16,397–16,410, doi:10.1029/93JC01504.

Hakkinen, S. (1999), Variability of the simulated meridional heat transport in the North Atlantic for the period 1951–1993, *J. Geophys. Res.*, *104*, 10,991–11,007, doi:10.1029/1999JC900034.

Hunkins, K., and J. A. Whitehead (1992), Laboratory simulation of exchange through Fram Strait, *J. Geophys. Res.*, *97*, 11,299–11,321, doi:10.1029/92JC00735.

Jakobsson, M., N. Cherkis, J. Woodward, R. Macnab, and B. Coakley (2000), New grid of Arctic bathymetry aids scientists and mapmakers, *Eos Trans. AGU*, *81*(9), 89.

Krishfield, R., J. Toole, A. Proshutinsky, and M. L. Timmermans (2008), Automated Ice-Tethered Profilers for seawater observations under pack ice in all seasons, *J. Atmos. Oceanic Technol.*, *25*, 2091–2105, doi:10.1175/2008JTECHO587.1.

Lazier, J. R. N. (1980), Oceanographic conditions at ocean weather ship bravo, 1964–1986, *Atmos. Ocean*, *18*, 227–238.

Lewis, E. L. (Ed.) (2000), *The Freshwater Budget of the Arctic Ocean*, NATO Sci. Ser., *2*, 623 pp., Kluwer Acad., Dordrecht, Netherlands.

Mosby, H. (1962), Water, salt and heat balance of the north Polar Sea and of the Norwegian Sea, *Geophys. Norv.*, *24*, 289–313.

Mysak, L. A., and S. A. Venegas (1998), Decadal climate oscillations in the Arctic: A new feedback loop for atmosphere-ice-ocean interactions, *Geophys. Res. Lett.*, *25*, 3607–3610, doi:10.1029/98GL02782.

Mysak, L. A., D. K. Manak, and R. F. Marsden (1990), Sea-ice anomalies observed in the Greenland and Labrador seas during 1901–1984 and their relation to an interdecadal Arctic climate cycle, *Clim. Dyn.*, *5*, 111–133, doi:10.1007/BF00207426.

Ostrom, W., J. Kemp, R. Krishfield, and A. Proshutinsky (2004), Beaufort Gyre freshwater experiment: Deployment operations and technology in 2003, *Tech. Rep. WHOI-2004–01*, 32 pp., Woods Hole Oceanogr. Inst., Woods Hole, Mass.

Overland, J. E. (2009), Meteorology of the Beaufort Sea, *J. Geophys. Res.*, *114*, C00A07, doi:10.1029/2008JC004861.

Perovich, D. K., T. C. Grenfell, B. Light, B. C. Elder, J. Harbeck, C. Polashenski, W. B. Tucker III, and C. Stelmach (2009), Transpolar observations of the morphological properties of Arctic sea ice, *J. Geophys. Res.*, *114*, C00A04, doi:10.1029/2008JC004892.

Proshutinsky, A. Y., and M. A. Johnson (1997), Two circulation regimes of the wind-driven Arctic Ocean, *J. Geophys. Res.*, *102*, 12,493–12,514, doi:10.1029/97JC00738.

Proshutinsky, A., R. H. Bourke, and F. A. McLaughlin (2002), The role of the Beaufort Gyre in Arctic climate variability: Seasonal to decadal climate scales, *Geophys. Res. Lett.*, *29*(23), 2100, doi:10.1029/2002GL015847.

Proshutinsky, A., R. Krishfield, and D. Barber (2009), Preface to special section on Beaufort Gyre Climate System Exploration Studies: Documenting key parameters to understand environmental variability, *J. Geophys. Res.*, *114*, C00A08, doi:10.1029/2008JC005162.

Rennermalm, A. K., E. F. Wood, S. J. Déry, A. J. Weaver, and M. Eby (2006), Sensitivity of the thermohaline circulation to Arctic Ocean runoff, *Geophys. Res. Lett.*, *33*, L12703, doi:10.1029/2006GL026124.

Reynolds, R. W., and T. M. Smith (1994), Improved global sea surface temperature analyses using optimal interpolation, *J. Clim.*, *7*, 929–948, doi:10.1175/1520-0442(1994)007<0929:IGSSTA>2.0.CO;2.

Richter-Menge, J. A., D. K. Perovich, B. C. Elder, K. Claffey, I. Rigor, and M. Ortmeyer (2006), Ice mass balance buoys: A tool for measuring and attributing changes in the thickness of the Arctic sea ice cover, *Ann. Glaciol.*, *44*, 205–210, doi:10.3189/172756406781811727.

Semtner, A. J. (1987), A numerical study of sea ice and ocean circulation in the Arctic, *J. Phys. Oceanogr.*, *17*, 1077–1099, doi:10.1175/1520-0485(1987)017<1077:ANSOSL>2.0.CO;2.

Serreze, M. C., A. P. Barrett, A. G. Slater, R. A. Woodgate, K. Aagaard, R. B. Lammers, M. Steele, R. Moritz, M. Meredith, and C. M. Lee (2006), The large-scale freshwater cycle of the Arctic, *J. Geophys. Res.*, *111*, C11010, doi:10.1029/2005JC003424.

Steele, M., R. Morley, and W. Ermold (2001), PHC: A global ocean hydrography with a high-quality Arctic Ocean, *J. Clim.*, *14*, 2079–2087, doi:10.1175/1520-0442(2001)014<2079:PAGOHW>2.0.CO;2.

Stroeve, J., M. M. Holland, W. Meier, T. Scambos, and M. C. Serreze (2007), Arctic sea ice decline: Faster than forecast, *Geophys. Res. Lett.*, *34*, L09501, doi:10.1029/2007GL029703.

Sturm, M., J. Holmgren, and D. K. Perovich (2002), Winter snow cover on the sea ice of the Arctic Ocean at the Surface Heat Budget of the Arctic Ocean (SHEBA): Temporal evolution and spatial variability, *J. Geophys. Res.*, *107*(C10), 8047, doi:10.1029/2000JC000400.

Talley, L. D., and M. S. McCartney (1982), Distribution and circulation of Labrador Sea water, *J. Phys. Oceanogr.*, *12*, 1189–1205, doi:10.1175/1520-0485(1982)012<1189:DACOLS>2.0.CO;2.

Timofeev, V. T. (1960), *Water Masses of the Arctic Basin* (in Russian), Gydrometeoizdat, Leningrad, Russia.

Timokhov, L., and F. Tanis (Eds.) (1997), *Joint U.S.-Russian Atlas of the Arctic Ocean* [CD-ROM], Environ. Res. Inst. of Mich., Ann Arbor, Mich.

Timokhov, L., and F. Tanis (1998), *Joint U.S.-Russian Atlas of the Arctic Ocean* [CD-ROM], Environ. Res. Inst. of Mich., Ann Arbor, Mich.

Walsh, J. E., and W. L. Chapman (1990), Arctic contribution to upper-ocean variability in the North Atlantic, *J. Clim.*, *3*, 1462–1473, doi:10.1175/1520-0442(1990)003<1462:ACTUOV>2.0.CO;2.

White, D., et al. (2007), The arctic freshwater system: Changes and impacts, *J. Geophys. Res.*, *112*, G04S54, doi:10.1029/2006JG000353.

Wohlleben, T., and A. J. Weaver (1995), Interdecadal climate variability in the subpolar North Atlantic, *Clim. Dyn.*, *11*, 459–467, doi:10.1007/BF00207195.

Woodgate, R. A., K. Aagaard, and T. J. Weingartner (2005), Monthly temperature, salinity, and transport variability of the Bering Strait through flow, *Geophys. Res. Lett.*, *32*, L04601, doi:10.1029/2004GL021880.

Yang, J., and J. C. Comiso (2007), An unexpected seasonal variability of salinity in the Beaufort Sea upper layer in 1996–1998, *J. Geophys. Res.*, *112*, C05034, doi:10.1029/2004JC002716.

Zubov, N. N. (1943), *Arctic Ice*, translated from Russian by U.S. Navy Oceanographic Office, 491 pp., U.S. Navy Electr. Lab., San Diego, Calif.

————————

E. Carmack, F. McLaughlin, W. J. Williams, and S. Zimmermann, Institute of Ocean Sciences, Fisheries and Oceans Canada, 9860 West Saanich Road, Sidney, BC V8L 4B2, Canada.

M. Itoh and K. Shimada, Japan Agency for Marine-Earth Science and Technology, 2-15 Natsushima, Yokosuka, Kanagawa 237-0061, Japan.

R. Krishfield, A. Proshutinsky, M.-L. Timmermans, and J. Toole, Woods Hole Oceanographic Institution, 266 Woods Hole Road, Woods Hole, MA 02543, USA. (aproshutinsky@whoi.edu)